

# UC Merced

## UC Merced Previously Published Works

### Title

Mucin O-glycans are natural inhibitors of *Candida albicans* pathogenicity

### Permalink

<https://escholarship.org/uc/item/60c3n6v2>

### Journal

Nature Chemical Biology, 18(7)

### ISSN

1552-4450

### Authors

Takagi, Julie  
Aoki, Kazuhiro  
Turner, Bradley S  
[et al.](#)

### Publication Date

2022-07-01

### DOI

10.1038/s41589-022-01035-1

Peer reviewed

Published in final edited form as:

Nat Chem Biol. 2022 July ; 18(7): 762–773. doi:10.1038/s41589-022-01035-1.

## Mucin O-glycans are natural inhibitors of *Candida albicans* pathogenicity

Julie Takagi<sup>1,2</sup>, Kazuhiro Aoki<sup>3</sup>, Bradley S. Turner<sup>1</sup>, Sabrina Lamont<sup>4</sup>, Sylvain Lehoux<sup>5</sup>, Nicole Kavanaugh<sup>1</sup>, Megha Gulati<sup>6,7</sup>, Ashley Valle Arevalo<sup>6,8</sup>, Travis J. Lawrence<sup>6,8,9</sup>, Colin Y. Kim<sup>1</sup>, Bhavya Bakshi<sup>3</sup>, Mayumi Ishihara<sup>3</sup>, Clarissa J. Nobile<sup>6,10</sup>, Richard D. Cummings<sup>5</sup>, Daniel Wozniak<sup>4</sup>, Michael Tiemeyer<sup>3</sup>, Rachel Hevey<sup>11,\*</sup>, Katharina Ribbeck<sup>1,\*</sup>

<sup>1</sup>Department of Biological Engineering, Massachusetts Institute of Technology, Cambridge, MA, USA

<sup>2</sup>Department of Biology, Massachusetts Institute of Technology, Cambridge, MA, USA

<sup>3</sup>Complex Carbohydrate Research Center, University of Georgia, Athens, GA, USA

<sup>4</sup>Departments of Microbial Infection and Immunity, Microbiology, The Ohio State University, Columbus, OH, USA

<sup>5</sup>Department of Surgery, Beth Israel Deaconess Medical Center, Harvard Medical School, National Center for Functional Glycomics, Boston, MA, USA

<sup>6</sup>Department of Molecular and Cell Biology, School of Natural Sciences, University of California Merced, Merced, CA, USA

<sup>8</sup>Quantitative and Systems Biology Graduate Program, University of California Merced, Merced, CA, USA

<sup>10</sup>Health Sciences Research Institute, University of California Merced, Merced, CA, USA

<sup>11</sup>Department of Pharmaceutical Sciences, University of Basel, Basel, Switzerland

### Abstract

Users may view, print, copy, and download text and data-mine the content in such documents, for the purposes of academic research, subject always to the full Conditions of use: <https://www.springernature.com/gp/open-research/policies/accepted-manuscript-terms>

\*Correspondence: [ribbeck@mit.edu](mailto:ribbeck@mit.edu), [rachel.hevey@unibas.ch](mailto:rachel.hevey@unibas.ch).

<sup>7</sup>Present address: Molecular Cell, Cell Press, Cambridge, MA, USA

<sup>9</sup>Present address: Oak Ridge National Laboratory, Oak Ridge, TN, USA

#### Author contributions

J.T. and K.R. designed the experiments. N.K. performed the RNA extraction for the mucin RNA Seq and preliminary experiments on the bacterial-fungal coculture. B.S.T. purified glycans. C.J.N, M.G., A.V.A., and T.J.L. performed and analyzed mucin RNA Seq. experiments. R.H. designed the synthetic approach and synthesized individual glycans. C.Y.K. performed a preliminary glycan analysis. S.Lamont and D.J.W. designed and performed murine experiments. B.B. and M.I. compiled bioinformatic parameters for glycan accessions and reporting. J.T. performed the *C. albicans* experiments. S.Lehoux and R.D.C. performed the preliminary glycan mass spectrometry experiments. K.A. designed and performed mass spectrometry of permethylated glycans. J.T., R.H., M.T. and K.R. wrote the manuscript.

#### Competing Interests

Clarissa J. Nobile is a cofounder of BioSynesis, Inc., a company developing diagnostics and therapeutics for biofilm infections. A patent application based on these results has been submitted by Massachusetts Institute of Technology and University of Basel with R.H., J.T., K.R. as inventors. All other authors declare no competing interests.

Mucins are large gel-forming polymers inside the mucus barrier that inhibit the yeast to hyphal transition of *Candida albicans*, a key virulence trait of this important human fungal pathogen. However, the molecular motifs in mucins that inhibit filamentation remain unclear, despite their potential for therapeutic interventions. Here, we determined that mucins display an abundance of virulence-attenuating molecules in the form of mucin *O*-glycans. We isolated and catalogued >100 mucin *O*-glycans from three major mucosal surfaces and established that they suppress filamentation and related phenotypes relevant to infection, including surface adhesion, biofilm formation, and cross-kingdom competition between *C. albicans* and the bacterium *Pseudomonas aeruginosa*. Using synthetic *O*-glycans we identified three structures (Core 1, Core 1+fucose, and Core 2+galactose) that are sufficient to inhibit filamentation with potency comparable to the complex *O*-glycan pool. Overall, this work identifies mucin *O*-glycans as host molecules with untapped therapeutic potential to manage fungal pathogens.

## Introduction

*Candida albicans* is an opportunistic fungal pathogen that asymptomatically colonizes the mucosal surfaces of most healthy humans<sup>1,2</sup>. Alterations to the mucus barrier and microbiota can lead to *C. albicans* overgrowth and infection, causing conditions such as oral thrush, vulvovaginal candidiasis, and life-threatening systemic candidiasis<sup>1,3</sup>. The scarcity of antifungal drug classes, their limited efficacy, toxicity, and the development of resistance<sup>4</sup> contribute to a mortality rate of ~40% in deep-seated candidiasis<sup>3</sup>, highlighting an urgent need for alternative treatments to fungal infections.

Targeting pathogenic mechanisms rather than growth represents an attractive approach for developing novel antimicrobial agents. The infection of diverse host niches is supported by a wide range of *C. albicans* virulence and fitness attributes, including the morphological yeast-to-hyphal transition (filamentation), adhesin expression, biofilm formation, and the secretion of hydrolytic enzymes that damage the underlying epithelium<sup>5</sup>. The yeast-to-hyphal transition is a major virulence factor<sup>5</sup> and is integral for robust biofilms, which are intrinsically resistant to treatment, posing a significant clinical challenge<sup>6</sup>. Strikingly, despite its potential for pathogenicity, *C. albicans* is accommodated in healthy mucus<sup>7</sup>, suggesting that mucus may underpin novel strategies for preventing *C. albicans* virulence.

Mucus is a complex viscoelastic secretion that coats all non-keratinized epithelial surfaces in the body that are exposed to and communicate with the external environment<sup>8</sup>. Much of the microbiota is housed in the mucus layer, serving as a protective barrier and microbial niche<sup>8,9</sup>. Mucins are the main structural component of mucus and play an integral role in attenuating virulence traits in various cross-kingdom pathogens, including *C. albicans*<sup>2,10</sup>. Mucin exposure suppresses *C. albicans* virulence phenotypes, including the formation of host-cell-penetrating hyphae<sup>10</sup>. However, the mechanisms through which mucins attenuate virulence in *C. albicans* remain unknown, impeding their application for therapeutic intervention.

To close this gap, we characterized the mechanism and biochemical motifs of mucins that suppress *C. albicans* virulence gene expression and phenotypes. By isolating and characterizing mucin-derived glycans across major mucosal surfaces, we determined that

mucin glycans repress *C. albicans* virulence traits including filamentation, adhesion, and biofilm formation and alter fungal–bacterial dynamics. We identified that specific Core-1- and Core-2-modified glycan structures within the mucin polymer suppress filamentation and downregulate filamentation-associated genes in *C. albicans*. These results elucidate the mechanisms by which healthy mucins attenuate *C. albicans* pathogenicity, suggesting therapeutic candidates for treating *C. albicans* infection without disrupting the microbiota (and potential evolution of antifungal resistance) that normally accompanies the killing of cells.

## Results

### Mucins share a conserved function in attenuating *C. albicans* virulence

While previous studies identified mucin polymers as candidates for managing *C. albicans* virulence *in vitro*<sup>10</sup>, it is unclear whether mucin activity persists in native and complex mucus or in the context of an intact immune system, which may indicate whether mucins are viable candidates for therapeutic intervention on mucosal surfaces. Here, we investigated mucus from three distinct sources (Extended Data Fig. 1a)—porcine intestinal mucus, porcine gastric mucus, and human saliva—representing model systems<sup>11–13</sup> for mucosal niches colonized by *C. albicans* (Fig. 1a). We quantified *C. albicans* adhesion to a polystyrene surface using fluorescence microscopy in medium with or without mucus. All three mucus types significantly decreased *C. albicans* adhesion *in vitro* (Extended Data Fig. 1b). Cell growth was similar with or without mucus (Extended Data Fig. 1c); thus, mucus shifts *C. albicans* to a planktonic state without affecting viability.

One candidate for mediating this function is mucin polymers, which suppress *C. albicans* adhesion *in vitro*<sup>10</sup>. To determine whether mucins are the dominant adhesion-suppressing factor in mucus, we removed high-molecular-weight components from porcine intestinal mucus using a centrifugal filter with a 100-kDa cutoff. The filtrate was less effective in preventing adhesion than whole mucus (Fig. 1b). Re-introducing the filtrate with 0.5% w/v MUC2, the predominant mucin in the intestinal tract, restored this effect and significantly decreased adhesion; similar results were observed for all three mucin types (Fig. 1b, Extended Data Fig. 1d,e). Thus, mucins from these mucosal surfaces are both necessary and sufficient to recapitulate the adhesion-suppressing effects of mucus.

To clarify how mucins regulate *C. albicans* physiology, we performed RNA sequencing on cells grown in RPMI medium with or without (0.5% w/v) MUC2 (intestinal mucin), MUC5B (salivary mucin), or MUC5AC (gastric/respiratory mucin), representing mucins secreted on mucosal surfaces abundantly colonized by *C. albicans* (Supplementary Data 1). Each mucin type elicited a specific gene-expression profile (Fig. 1c,d), with 262 downregulated and 343 upregulated genes ( $P < 0.05$ ) shared among the three transcriptional profiles (Fig. 1e). Filamentation- and adhesion-regulating pathways were enriched in the shared downregulated genes (Supplementary Data 2). Notably, all three mucins caused the downregulation of various virulence-associated genes (Fig. 1f). Consistent with previous observations<sup>10</sup>, inoculation of *C. albicans* in RPMI medium caused the formation of extensive hyphae, while mucin-exposed cells were predominantly in the round yeast form or formed short chains resembling pseudohyphae (Fig. 1g, Extended Data Fig.

2a). The upregulated pathways were enriched in genes encoding cellular amino-acid and small-molecule biosynthetic and metabolic processes (Supplementary Data 2). *C. albicans* metabolism plays a central role in biofilm formation and hyphal morphogenesis<sup>14</sup>; thus, metabolic changes may correlate with virulence suppression. Together, these data indicate that mucins across various mucosal surfaces downregulate virulence-associated gene expression and phenotypes, providing rich sources of bioactive molecules for regulating *C. albicans*.

To investigate the roles of mucins in the context of an intact immune system (Fig. 1h), we infected murine puncture wounds with *C. albicans*, topically treated the wounds with 0.5% MUC2, and quantified the fungal burden over time in colony-forming units (CFUs). While the fungal burden on day 5 and 7 did not differ between MUC2 and mucin-free treatment, exposure to MUC2, but not mucin-free mock treatment, caused a significant CFU reduction 7 days post-infection compared to day 5 of infection (Fig. 1i). This enhanced *C. albicans* clearance is likely not due to direct killing by MUC2 because mucins do not alter growth (Fig. 1j)<sup>10</sup>. Rather, mucins may facilitate fungal clearance by attenuating *C. albicans* pathogenicity, thus supporting host defense mechanisms to reduce the fungal burden in the wound.

### Mucin glycans act via Nrg1 to prevent filamentation

Mucin glycans are promising molecules for regulating host–microbe interactions: they serve as nutrients<sup>15</sup>, microbial binding sites<sup>8</sup>, and signaling molecules<sup>18,19</sup>. To determine whether mucin glycans mediate virulence suppression, we isolated glycans via non-reductive, alkaline  $\beta$ -elimination, which preserved the structural heterogeneity of glycan chains, yielding a library of glycans released from MUC5AC (Fig. 2a). We analyzed the released glycans as permethylated derivatives using nanospray-ionization multi-dimensional mass spectrometry (NSI-MSn, ThermoFisher Orbitrap Discovery) to characterize structural topology features beyond simple monosaccharide composition (Fig. 2b, Supplementary Table 1). We identified >80 glycan structures, including isobaric glycans with distinct structural characteristics. Negative-mode NSI-MSn indicated sulfation on 34 of these glycans. The MUC5AC glycan pool was dominated by Core-1- and Core-2-type O-glycan structures that were partially modified by fucose, possessed multiple LacNAc repeats, and were only sparsely capped by sialic acid (Fig. 2c). Sulfation was most abundant on non-sialylated Core-2-type O-glycans with a single fucose (Supplementary Table 2).

To determine whether the mucin glycan pool can replicate mucin-induced virulence suppression, we performed RNA sequencing of *C. albicans* in medium with or without 0.1% w/v MUC5AC glycans. A pooled library of MUC5AC glycans triggered global gene expression changes, with 233 and 308 genes significantly upregulated and downregulated, respectively, compared with cells grown in medium alone ( $P < 0.05$ ; Fig. 2d, Supplementary Data 3). Similar to intact mucins, MUC5AC glycans upregulated the transcription of amino-acid biosynthetic and metabolic processes (Supplementary Data 4) and downregulated pathways associated with filamentation, biofilm formation, and interspecies interactions (Fig. 2e).

Over 20% of the downregulated genes were associated with filamentous growth, which was suppressed by intact mucins (Supplementary Data 4). We found that isolated MUC5AC glycans suppressed filamentation across the three medium conditions without altering growth, while medium alone supported the formation of extensive hyphae (Fig. 2f,g, Extended Data Fig. 2b). Addition of the monosaccharides found in mucins did not suppress filamentation or alter the expression of signature hyphal-specific (*UME6*, *HGCI*)<sup>20,21</sup> or yeast-specific (*YWPI*)<sup>22</sup> genes relative to medium alone (Fig. 2h). We detected gene expression changes 30 min after exposure to MUC5AC glycans, which intensified over 4 h (Fig. 2i). Filamentation suppression was visualized 4 h after hyphal induction (Extended Data Fig. 2c) and the round yeast morphology was maintained over 8 h (Fig. 2f), suggesting a prolonged glycan response. Further, we detected a dose-dependent effect of mucin glycans, with potent filamentation suppression occurring at concentrations below those of mucosal surfaces (Fig. 2j, Extended Data Fig. 3). Together, these data demonstrate that complex glycan structures are critical for retaining *C. albicans* in a host-compatible yeast state and may signal a healthy mucosal environment.

Hyphal morphogenesis in *C. albicans* is induced by environmental signals acting via multiple signaling cascades, including a cAMP-dependent pathway and a MAPK pathway (Fig. 3a)<sup>23</sup>. Our RNA-sequencing data revealed that the transcription of many filamentation activators and key outputs of these pathways (including hyphal-specific proteins Ume6, Eed1, and Hgc1<sup>24</sup>) were significantly downregulated in the presence of mucin glycans (Fig. 3a, Extended Data Fig. 4a). Hyphal-specific gene expression is negatively regulated by a protein complex consisting of the general transcriptional corepressor Tup1 and DNA-binding proteins Nrg1 or Rfg1<sup>24</sup>. The transcription of *NRG1*, a major transcriptional repressor of filamentation, increased in the presence of mucin glycans (Fig. 3a). Thus, mucin glycans may inhibit filamentation by regulating transcriptional activators and/or repressors, which play prominent roles in the yeast-to-hyphal transition<sup>23</sup>.

To assess whether mucin glycans suppress hyphal formation by preventing activation of the major transcriptional activators of filamentation, we screened mutants that constitutively activate major positive filamentation regulators (Ras1, Cph1, and Efg1) for the filamentation-suppression response to mucin glycans. Ras1 cycles between inactive and active states. The *RAS1*<sup>G13V</sup> strain is locked in an active state, leading to hyperfilamentation<sup>25</sup>. If mucin glycans act upstream or directly via Ras1 activation, the dominant active *RAS1*<sup>G13V</sup> strain should remain filamentous in the presence of mucin glycans, being unable to respond to mucin glycans. However, in the presence of mucin glycans, cells from both the *RAS1*<sup>G13V</sup> strain and wild-type strain retained the yeast morphology (Fig. 3b, Extended Data Fig. 2c,d), suggesting that this function does not depend on Ras1 activation.

To determine whether mucin glycans act via the cAMP-PKA pathway, we tested whether mucin glycans suppress filamentation in a strain with a phosphomimetic mutation controlled by the glucose-repressible *PCK1* promoter<sup>26,27</sup> (*PCKpr-efg1-T206E*), which simulates constitutive signaling of Efg1, a downstream transcription factor in the cAMP-PKA pathway<sup>23</sup>. In the presence of mucin glycans, cells from a constitutively expressed Efg1 transcription factor transitioned to a yeast morphology, as observed for the wild-type strain

in Spider medium (Fig. 3b, Extended Data Fig. 2c,e), suggesting that the filamentation suppression of mucin glycans is independent of the cAMP-PKA pathway. To determine whether mucin glycans act via the MAPK pathway, we tested filamentation suppression in a strain over expressing Cph1 (*prADHI-CPHI*). In the presence of mucin glycans, cells overexpressing Cph1 remained in the yeast form (Fig. 3b) at levels comparable to those of the wild-type strain (Extended Data Fig. 2c,d), indicating that mucin glycans suppress filamentation independently of the MAPK pathway. Thus, mucin glycans do not act directly via the major transcriptional activators of hyphal induction to suppress filamentation; instead, they likely act downstream of Cph1 and Efg1 or via alternate pathways.

To explore alternate regulation pathways, we examined whether mucin glycans act via transcriptional repressors of filamentation, which inhibit the yeast-to-hyphal transition<sup>23</sup>. We focused on *NRG1* and *TUP1*, as their loss leads to constitutive filamentation and upregulation of hyphal genes, even in non-inducing conditions<sup>28</sup>. Specifically, 30 min after exposure to mucin glycans (Fig. 3c), expression of Nrg1 was upregulated, which continued throughout an 8-h time course (Fig. 3a). If filamentation suppression depends on Nrg1 or Tup1, those mutant strains should remain filamentous in the presence of mucin glycans. Indeed, opposed to the wild-type strain (Extended Data Fig. 2c), upon exposure to mucin glycans, cells lacking *NRG1* or *TUP1* were constitutively filamentous in the presence or absence of mucin glycans (Fig. 3d), suggesting that mucin glycans block hyphal formation in an Nrg1/Tup1-dependent manner.

To further explore this function of mucin glycans, we performed RNA sequencing of the wild-type strain and *Δnrg1* mutant strain after 2 h in the presence or absence of mucin glycans to detect early transcriptional changes during hyphal morphogenesis. In the wild-type strain, mucin glycans downregulated 45 and upregulated 64 genes ( $P < 0.05$ ) after 2 h (Fig. 3e, Supplementary Data 5). The transcription of several hyphal-specific genes (*ALS3*, *HWPI*, *EFG1*, and *HGC1*) was downregulated; further, *YWPI*, a marker for yeast cells, was upregulated (Fig. 3e). We also detected downregulation of genes involved in ion regulation, white–opaque regulation, and amino-peptidase activity (Fig. 3e). However, in the *Δnrg1* mutant strain, only 22 genes were differentially expressed (Fig. 3e, Supplementary Data 6). Several genes involved in ion homeostasis were differentially downregulated in the *Δnrg1* mutant strain and wild-type strain (Fig. 3e), suggesting that these changes constitute general responses to mucin glycans, independent of morphology. The hyphal-associated genes that were downregulated in the wild-type strain were unchanged in the *Δnrg1* mutant strain (Fig. 3f), consistent with the observation that the *Δnrg1* mutant strain remains filamentous in the presence of mucin glycans (Fig. 3d). These observations imply that mucin glycans act via Nrg1 to downregulate the expression of hyphal-specific and other virulence-associated genes.

### Mucin glycans regulate group-level behavior

A major virulence attribute of *C. albicans* is its ability to form robust biofilms<sup>6</sup>. Biofilm cells are highly resistant to conventional antifungal therapeutics and the host immune system, making them highly pathogenic<sup>6</sup>. In *C. albicans*, biofilm development requires six master transcriptional regulators (Efg1, Tec1, Bcr1, Ndt80, Brg1, and Rob1)<sup>29</sup>. The first step in

biofilm formation involves cell adherence to a surface, mediated by the master regulator Bcr1 and its downstream target genes<sup>30</sup>.

We observed that MUC5AC glycans significantly downregulated the transcription of several genes involved in adherence and biofilm initiation, while equivalent amounts of monosaccharides had no effect (Fig. 4a, Supplementary Data 3). By inoculating yeast cells into medium with or without (0.1% w/v) mucin glycans and visualizing surface adherence, we found that mucin glycans significantly reduced cell attachment, while equivalent amounts of monosaccharides had no effect (Fig. 4b,c).

After initial adherence and biofilm initiation, the next step in biofilm formation is biofilm maturation, where hyphal cells grow and all cells become encased in extracellular matrix<sup>29</sup>. Our RNA-sequencing data revealed significant downregulation of several transcriptional regulators of biofilm maturation, including genes encoding Efg1, Tec1, Brg1, and Rob1 (Extended Data Fig. 4a,b)<sup>30</sup>. To investigate *C. albicans* biofilm formation, we visualized biofilms formed on the bottom of polystyrene plates after 24 h of growth. *C. albicans* typically forms biofilms consisting of yeast, hyphae, and pseudohyphae cells; however, in the presence of MUC5AC glycans, only a layer of yeast-form cells was present on the plate surface (Fig. 4d), with more cells remaining in the yeast non-adhered (planktonic) state compared with the results observed for medium only (Fig. 4d,e, Extended Data Fig. 4c).

In a host, *C. albicans* is generally part of a larger multispecies microbial community<sup>6,31</sup>. We found that genes involved in microbial interspecies interactions are differentially regulated by mucin glycans (Supplementary Data 4), suggesting that mucins influence microbial community dynamics. *C. albicans* is often found in the presence of the bacterial pathogen *Pseudomonas aeruginosa*, both as part of the normal microbiota and during infection<sup>31</sup>. *In vitro* work has shown that these two microbes have an antagonistic relationship when grown together in *C. albicans* filamentation-inducing conditions<sup>32</sup>, where *P. aeruginosa* forms biofilms on *C. albicans* hyphal cells and secretes small molecules that result in fungal cell death (Fig. 4f). Consistent with previous work, *P. aeruginosa* does not adhere to or kill *C. albicans* yeast cells when these species are grown together in non-filamentation-inducing conditions (Fig. 4f)<sup>33</sup>.

Because mucins suppress filamentation (Fig. 1g)<sup>10</sup>, we hypothesized that in filamentation-inducing conditions, mucin glycans would increase the viability of *C. albicans* in coculture with *P. aeruginosa*. As previously reported<sup>32</sup>, cocultures grown under filamentation-inducing conditions in the absence of mucin glycans showed reduced *C. albicans* CFUs and eventual eradication of *C. albicans* cells (Fig. 4g). Addition of mucin glycans delayed *C. albicans* eradication (Fig. 4g), indicating that mucin glycans protect *C. albicans* against *P. aeruginosa*. Therefore, mucin glycans may influence microbial population dynamics by modulating *C. albicans* morphogenesis.

To determine whether filamentation suppression is the dominant factor promoting microbial coexistence, we cocultured the *C. albicans* / *nrg1* mutant strain, which remains filamentous in the presence of mucin glycans (Fig. 3d, Extended Data Fig. 4d,e), with *P. aeruginosa* in the presence or absence of mucin glycans. The increased viability of *C.*

*albicans* in the presence of mucin glycans was eliminated in the *nrg1* mutant strain (Fig. 4h), indicating that filamentation-suppression effects confer protection from *P. aeruginosa*. These results suggest that mucin glycans may influence microbial communities and inhibit a range of virulence behaviors.

### Mucins display a plethora of glycans with regulatory potential

To determine the glycan structures regulating *C. albicans* physiology and the therapeutic potential of novel glycan-based drugs for *C. albicans* infection, we screened mucin glycan libraries for filamentation suppression. Glycans isolated from human saliva (MUC5B), porcine gastrointestinal mucus (MUC2), and porcine gastric mucin (MUC5AC) all suppressed filamentation (Fig. 5a), suggesting that these mucin-derived glycans are sufficient to recapitulate the filamentation-suppression response in *C. albicans*.

To distinguish unique and shared structural features, we used NSI-MSn to analyze released, permethylated glycans from these three mucin pools (Methods, Extended Data Fig. 5). We identified glycans at 83 distinct mass/charge (*m/z*) ratios, approximately 1/3rd of which produced MS fragmentation, indicating the presence of 2–3 isomeric glycan structures (Fig. 5b, Supplementary Table 3). Thus, the full glycan diversity of these mucin pools exceeds the number of discrete *m/z* values detected by NSI-MSn. These glycans are predominantly characterized by the presence of a HexNAc (GalNAc) at their reducing terminal. This GalNAc, in O-linkage to serine or threonine amino acids of the mucin protein backbone, provides a foundation upon which a set of structurally distinct glycan core types are built; the core structures are extended to longer, more complex glycan structures depending on the repertoire of glycosyltransferases expressed in the tissue and species of origin. The majority of all three glycan pools consisted of glycans built on Core 1 (Gal $\beta$ 1-3GalNAc $\alpha$ 1-Ser/Thr) or Core 2 (Gal $\beta$ 1-3(GlcNAc $\beta$ 1-6)GalNAc $\alpha$ 1-Ser/Thr) structures, while the Tn antigen (GalNAc $\alpha$ 1-Ser/Thr) or glycans built on Core 3 (GlcNAc $\beta$ 1-6GalNAc $\alpha$ 1-Ser/Thr) and Core 4 (GlcNAc $\beta$ 1-3(GlcNAc $\beta$ 1-6)GalNAc $\alpha$ 1-Ser/Thr) structures contributed <10% for each glycan pool (Fig. 5c). Of these 83 glycan compositions, 51 were monosulfated and 20 were disulfated; the most abundant sulfated O-glycans of MUC2 and MUC5AC were Core-2-type, while the most abundant sulfated O-glycans of MUC5B were Core-1- and O-Man-type (Supplementary Table 2). MUC5AC and MUC5B glycans were more complex than MUC2 glycans (Fig. 5b, Supplementary Table 3). Specifically, >60% of MUC2 glycans were detected as the Core-1 disaccharide (glycan #2; Fig. 5b, Supplementary Table 3) or Core 1 modified with a single additional monosaccharide (Fuc or sialic acid; glycans #3 and 4, respectively), compared with <35% for MUC5AC and MUC5B.

Beyond the core structures, 23% and 15% of MUC5AC and MUC5B glycans, respectively, were more than seven sugars long, versus <3% of MUC2 glycans (Supplementary Table 3). The shortened length of MUC2 glycans may result from degradation through microbial feeding or differences in endogenous glycosyltransferase expression levels in the intestinal tract<sup>15</sup>. Consistent with previous reports<sup>18,34</sup>, mucin glycans from all three sources were heavily fucosylated, with >35% of structures containing at least one fucose, with minimal sialylation (Fig. 5d). MUC5AC yielded the highest abundance of non-fucosylated and asialo glycans (i.e., uncapped glycans), while MUC5B and MUC2 glycans were the most

fucosylated and most sialylated, respectively. These capping residues (Fuc and sialic acid) can block the extension of core structures by limiting the addition of *N*-acetylglucosamine (LacNAc) units. Thus, the glycan collection prepared from MUC5AC had the highest abundance of LacNAc repeats. We detected several glycan structural elements or motifs with known roles in immunorecognition (e.g., LacNAc, LacdiNAc, Lewis X, GalGal)<sup>35</sup> or cell adhesion (e.g., O-Man) as minor components of all three preparations (Fig. 5e); thus, these structures may contribute to immunomodulatory activities. Despite substantial overlap in the glycan structures among the three mucin glycan pools (Fig. 5b, Supplementary Table 3), differences in mucin glycan identity and length likely arise from niche-specific selective preferences that have coevolved to influence the structural and functional properties of the mucus barrier.

### Synthetic Core-1 and Core-2 structures suppress filamentation

Because glycan structure compositions vary across mucin types, we focused on glycan structures that were highly abundant across the mucin species examined here. In total, six glycan structures (Fig. 5f, Supplementary Table 3) were shared among all three mucin glycan pools and together represented >40% of the total glycan profile in each sample (Fig. 5f), highlighting them as candidates for virulence-attenuating activity. To date, most known mucin glycan structures have not been associated with clearly delineated functions.

Rather than fractionating glycan pools down to the single-glycan level, which poses technical challenges<sup>36</sup>, we developed a synthetic approach to obtain these six highly abundant mucin glycans (Fig. 6a, Supplementary Note). We first focused on Core 1 (**1**) and Core 2 (**2**), which constitute 40% of total mucin glycans (Supplementary Table 3). Neither Core 1 nor Core 2 showed toxic effects, as measured by *C. albicans* growth at a concentration of 0.1% (w/v), an effective concentration for filamentation suppression in the mucin glycan pool (Fig. 6b). To determine whether Core 1 and Core 2 have a similar regulatory capacity as the complex glycan pool, we tested their ability to regulate two signature proteins, the yeast-wall protein Ywp1 and the filamentation-associated cytotoxin Ece1, whose genes were strongly up- and downregulated, respectively, by the native mucin glycan pool (see Fig. 2). RT-qPCR revealed that Core 1 and Core 2 individually upregulated *YWPI* expression at 0.1% (w/v) to a similar degree as the intact mucin pool, and a concentration increase to 0.4% (w/v) did not significantly alter *YWPI* expression (Fig. 6c). Moreover, Core 1 and Core 2 both suppressed *ECE1* expression at 0.1% and 0.4%, albeit less strongly than the mucin glycan pool (Fig. 6c). By contrast, an equal-parts mixture of the mucin monosaccharide components did not change gene expression at corresponding concentrations (Fig. 6c). Thus, both Core 1 and Core 2 regulate these two genes with similar potency as the native glycan pool.

To elucidate the role of glycan composition, we tested the effects of four modified Core structures: Core 1+fucose (**3**), Core 1+sialic acid (**4**), Core 2+fucose (**5**), and Core 2+galactose (**6**) (Fig. 6a). These four glycans all transcriptionally upregulated *YWPI* while downregulating *ECE1*, similar to their unmodified Core counterparts (Fig. 6d,e). The addition of fucose to Core 1 and Core 2 did not measurably alter the ability of these structures to up- or downregulate the two signature genes (Fig. 6d,e); the addition

of galactose did not significantly alter Core 2 activity (Fig. 6e). However, the addition of sialic acid dampened the gene regulatory response of Core 1 (Fig. 6d). Exploring a broader range of filamentation-associated genes, we observed that all six synthetic glycans possessed a sliding range of bioactivity, rather than an on/off response: Core 1, Core 1+fucose, and Core 2+galactose showed the strongest suppression of filamentation-associated genes, while Core 1+sialic acid exhibited the weakest effect (Fig. 6f).

The phenotypic filamentation assay confirmed this conclusion: while medium alone supported the formation of extensive hyphal filaments, Core 1, Core 1+fucose, and Core 2+galactose most potently blocked filamentation, as evidenced by the predominance of yeast cells in culture with these structures compared with the monosaccharide pool and medium alone (Fig. 6g, Extended Data Fig. 2f). Core 1+sialic acid was less effective at suppressing filamentation, despite partially downregulating the transcription of filamentation-associated genes (Fig. 6d,g).

## Discussion

Research on mucus has traditionally focused on the role of mucins as scaffolding polymers. Here, we show that mucin *O*-glycans potently inhibit a range of virulence behaviors, which could be leveraged for therapeutic applications. Specifically, we show that mucin glycans across three major niches are potent regulators of *C. albicans* filamentation (Fig. 2) that block hyphal formation through Nrg1 (Fig. 3) and regulate community behavior (Fig. 4). These insights demonstrate the wealth of biochemical information and regulatory power housed within mucus and may inform diagnostic strategies for treating and preventing infection.

By characterizing bioactive glycans across mucin types, we identified and synthesized prominent Core-1- and Core-2-modified structures commonly found across mucosal surfaces. We demonstrated that Core 1, Core 2+galactose, and Core 1+fucose individually suppress filamentation at potencies comparable to those of native mucins. Our findings highlight that *O*-glycans can control virulence traits (Fig. 6) without killing the microbe, which may prevent the evolution of drug resistance. Many well-known small-molecule drugs, such as antibiotics and anticancer agents<sup>37</sup>, naturally contain glycans as part of their core structure and/or sugar side chain. Therefore, the discovery of *O*-glycans that attenuate *C. albicans* virulence may lead to novel glycan-based or glycan-mimetic therapeutics that enhance, or even replace, current antifungals. Native glycans, which are unconjugated to larger macromolecules, are generally ineffective as small-molecule pharmaceuticals due to their inherently poor pharmacokinetic properties<sup>38</sup>. By identifying the most bioactive mucin *O*-glycans, we can establish the precise glycan epitopes required for activity to design glycomimetic structures that retain activity while exhibiting improved drug-like properties. For example, glycan hydroxyl groups or post-synthetic modifications that are not necessary for activity can be chemically modified or eliminated to improve overall drug-likeness<sup>39</sup>. Additionally, smaller glycan epitopes should be more amenable to larger-scale production. Frequently, small glycans with biological activity gain potency when presented as multivalent conjugates on a defined backbone. Identifying minimal functional epitopes

of mucin glycans may lead to conjugates with enhanced efficacies, which may mimic the multivalent glycan presentation offered by endogenous mucin proteins.

Given the complexity and diversity of mucin glycans<sup>18,34</sup> and dynamic glycosylation changes based on cell type<sup>40</sup>, developmental stage<sup>41</sup>, and disease state<sup>42</sup>, structural changes in host signals may activate or inhibit the function of specific *O*-glycans. Accordingly, we determined that Core 1, Core 1+fucose, and Core 2+galactose effectively suppress filamentation, while Core 1+sialic acid significantly dampens this response. Hence, sialic acid, which is ubiquitously expressed on host cells<sup>43</sup>, may have an unappreciated role in modulating virulence. We posit that changes in glycosylation in disease states may mask or eliminate mucins' protective functions. We conclude that the presentation of complex glycan structures in mucus contributes to a healthy mucosal environment, while degradation or modification of mucin glycans may trigger *C. albicans* to transition from commensal to pathogenic.

The receptors involved in sensing mucin glycans, leading to *NRG1* upregulation, remain unknown. Nrg1 regulation is temporally coordinated by two central signaling pathways mediating cell growth, leading to transient *NRG1* downregulation and degradation of Nrg1 protein followed by occlusion of Nrg1 from hyphal-specific promoters that sustain hyphal development<sup>24</sup>. Mucin glycans may potentially function as ligands to mimic nutrient signaling pathways or may bind directly to *C. albicans* adhesins, thus modulating morphogenesis<sup>44</sup>. Uncovering the receptors involved in sensing mucin glycans and the pathways regulated by glycans will elucidate how *C. albicans* senses its host environment and how these cues regulate microbial antagonism, microbial community composition, and pathogenesis.

## Methods

### *C. albicans* strains and media

Strains were maintained on YPD agar (2% Bacto peptone, 2% glucose, 1% yeast extract, 2% agar) and grown at 30 °C. Single colonies were inoculated into YPD broth and grown with shaking overnight at 30 °C prior to each experiment. Experiments were performed with Gibco RPMI 1640 medium (catalog number 31800-089; Life Technologies) buffered with 165 mM 3-(*N*-morpholino)propanesulfonic acid (MOPS) and supplemented with 0.2% NaHCO<sub>3</sub> and 2% glucose; YPD medium with 10% fetal bovine serum; GlcNAc medium (0.5% *N*-acetylglucosamine, 0.5% peptone, 0.3% KH<sub>2</sub>PO<sub>4</sub>); Spider medium (1% nutrient broth, 1% D-mannitol, 2 g K<sub>2</sub>HPO<sub>4</sub>, 50 mg/mL arginine, 10 mg/mL histidine, and 50 mg/mL tryptophan); or Lee's medium<sup>45</sup>. Growth curves were performed in Synthetic Defined (SD) + 0.004% (w/v) L-Arginine + 0.0025% (w/v) L-Leucine media with 2% glucose.

The *C. albicans* reference strains used in this study were SC5314 and HGFP3. Strain HGFP3 was constructed by inserting the *GFP* gene next to the promoter of *HWPI*, a gene encoding a hyphal cell wall protein, in SC5314; this strain was provided by E. Mylonakis (Massachusetts General Hospital, Boston, MA) with the permission of P. Sundstrom. Homozygous deletion strains were obtained from the transcriptional

factor deletion collection and were provided by the Fungal Genome Stock Center (<http://www.fgsc.net/>). The following *C. albicans* strains used for pathway analyses were gifts from Paul Kauman (University of Massachusetts, Medical School): AV55 (ura3:: $\lambda$ imm434/ura3:: $\lambda$ imm 434; LEU2::pCK1-efg1- T206E::URA3); DH409 (ura3:: $\lambda$ imm434/ura3; ras1-G13V); and CDH72-1 (ura3/ura3 cph1 ::hisG/cph1 ::hisG; ADH1prCPH1).

### Collection of human saliva

Submandibular saliva was collected from healthy human volunteers using a custom vacuum pump, pooled, centrifuged at 2,500 x *g* for 5 min, and 1 mM of phenylmethylsulfonylfluoride was added. Samples of human saliva were collected after explaining the nature and possible consequences of the studies, obtaining informed consent, and receiving approval from the institutional review board and Massachusetts Institute of Technology's Committee on the Use of Humans as Experimental Subjects under protocol no. 1312006096.

### Mucin purification

This study used native porcine gastric mucins (MUC5AC), porcine intestinal mucins (MUC2), and human salivary mucins (MUC5B), which differ from industrially purified mucins in their rheological properties and bioactivities<sup>10,46</sup>. Native mucins were purified as described previously<sup>10,18</sup>. In brief, mucus was scraped from fresh pig stomachs and intestines and solubilized in sodium chloride. Insoluble material was removed via ultracentrifugation at 190,000 x *g* for 1 h at 4 °C (Beckman 50.2 Ti rotor with polycarbonate bottles). Submandibular saliva was collected from human volunteers as described above using a custom vacuum pump, pooled, centrifuged, and protease inhibitors were added<sup>10</sup>. Mucins were purified using size-exclusion chromatography on separate Sepharose CL-2B columns. Mucin fractions were then desalted, concentrated, and lyophilized for storage at -80 °C. Lyophilized mucins were reconstituted by shaking them gently at 4 °C overnight in the desired medium.

Mass spectrometry is routinely used to monitor the composition of purified mucin extracts. This type of analysis has shown that mucin extracts purified from porcine stomach mucus, for example, are composed predominantly of MUC5AC, with small quantities of MUC2, MUC5B, and MUC6, as well as histones, actin, and albumin<sup>47</sup>.

### Isolation of mucin oligosaccharides

We applied non-reductive alkaline  $\beta$ -elimination ammonolysis to dissociate non-reduced glycans from mucins as described previously<sup>18,48</sup>. Purified mucins were dissolved in ammonium hydroxide saturated with ammonium carbonate and incubated at 60 °C for 40 h to release oligosaccharide glycosylamines and partially deglycosylated mucins. Volatile salts were removed using repeated centrifugal evaporation and the oligosaccharide glycosylamines were separated from residual deglycosylated mucins via centrifugal filtration through 3–5 kDa molecular weight cut-off membranes (Amicon Ultracel) in accordance with the manufacturer's instructions. The resulting oligosaccharide glycosylamines were converted to reducing oligosaccharide hemiacetals via treatment with boric acid. Residual boric acid was removed via repeated centrifugal evaporation

from methanol. Oligosaccharides were further purified using solid-phase extraction using Hypercarb mini-columns (ThermoFisher) and residual solvents were removed through centrifugal evaporation.

### Analysis of mucin O-glycan profiles

Glycans released from MUC2, MUC5B, and MUC5AC were permethylated and analyzed by nanospray ionization tandem mass spectrometry (NSI-MS) following direct infusion into a linear/orbital hybrid ion trap instrument (Orbitrap-LTQ Discovery, ThermoFisher) operated in positive ion mode for non-sulfated glycans or in negative mode for the detection of sulfated glycans. The permethylated O-glycans were dissolved in 1 mM sodium hydroxide in methanol/water (1:1) for infusion at a syringe flow rate of 0.60  $\mu\text{l}/\text{min}$  and capillary temperature set to 210  $^{\circ}\text{C}$ <sup>49</sup>. For fragmentation by collision-induced dissociation (CID) in MS/MS and MS<sup>n</sup>, a normalized collision energy of 35-40% was applied. Detection and relative quantification of the prevalence of individual glycans was accomplished using the total ion mapping (TIM) functionality of the Xcalibur software package version 2.0 (ThermoFisher) as previously described<sup>49</sup>. For TIM, the  $m/z$  range from 600 to 2000 was automatically scanned in successive 2.8 mass unit windows with a window-to-window overlap of 0.8 mass units, which allowed the naturally occurring isotopes of each glycan species to be summed into a single response, thereby increasing detection sensitivity. Most glycan components were identified as singly, doubly, and/or triply charged, sodiated species ( $M + \text{Na}$ ) in positive mode or as singly or doubly charged ( $M - \text{H}$ ) species in negative mode. Charge states for each glycan were deconvoluted manually and summed for quantification. Structural representations of mucin glycans were based on topologic features detected upon CID fragmentation and knowledge of O-glycan biosynthetic pathways. Approximately 33% of the  $m/z$  values reported here were associated with 2 or 3 isomeric glycan structures. NSI-MS/MS and MS<sup>n</sup> were used as needed to assign isomeric heterogeneity at each of these  $m/z$  values. For purposes of representing and comparing the heterogeneity of the glycan profile associated with each mucin, the signal intensity associated with an  $m/z$  value comprised of more than one glycan was assigned to the most abundant glycan structure among the isomers. Graphic representations of glycan monosaccharide residues are consistent with the Symbol Nomenclature For Glycans (SNFG) as adopted by the glycomics and glycobiology communities. Glycomics data and metadata were obtained and are presented in accordance with MIRAGE standards and the Athens Guidelines<sup>50</sup>. GlyTouCan accessions were retrieved from the GlyTouCan repository through GlyGen for glycan instances in which accessions already existed. If new accessions were required for glycans not previously placed in the repository, the desired structural representations were generated in GlycoGlyph and submitted directly to GlyTouCan for registration<sup>51</sup>. All raw mass spectrometric data related to mucin glycan profiles were deposited at GlycoPost<sup>52</sup>. Heatmap and other data analysis was performed on extracted signal intensities using Prism GraphPad and Excel software.

### Filamentation assay

Hyphal growth of *C. albicans* was induced by diluting cells to  $\text{OD}_{600}=0.05$  into pre-warmed hyphae-inducing medium as indicated and incubating at 37  $^{\circ}\text{C}$  (200 rpm) in a glass-bottom, 96-well plate. Cells were grown in hyphae-inducing medium for several hours, as described in the figure legends. Images were acquired with a confocal laser scanning microscope

(LSM 800; Zeiss) equipped with a  $\times 63/1.4$  NA oil-immersion or a 25x objective. Images were analyzed using Zeiss ZEN v.2.1. Representative micrographs are shown.

### RNA extraction

For the extraction of the RNA of *C. albicans* grown in the presence or absence of mucins, 1 mL of RPMI or 0.5% w/v MUC2, MUC5AC, or MUC5B in RPMI was inoculated with 10  $\mu$ L of an overnight culture of strain SC5314 and incubated in a culture tube at 37 °C with shaking (180 rpm) for 8 h. Total RNA was extracted using the Epicentre MasterPure Yeast RNA Purification Kit and treated with Sigma-Aldrich AMPD1 amplification-grade DNase I.

For RNA extraction from *C. albicans* grown in the presence or absence of mucin glycans, 100  $\mu$ L of RPMI or 0.1% w/v MUC5AC glycans in RPMI were inoculated with a 1:50 dilution of an overnight culture of strain SC5314 and incubated at 37 °C for the time indicated. Total RNA was extracted with the MasterPure RNA Purification Kit (Lucigen) and residual DNA was removed using the Turbo DNA-free kit (Ambion). The integrity of the total RNA was assessed using an Agilent 2100 Bioanalyzer (Agilent Technologies). rRNA was removed using the Ribo-Zero rRNA Removal Kit (Yeast; Epicentre).

### RNA sequencing

For RNA sequencing of *C. albicans* grown in mucins, poly(A) RNA was isolated from total RNA via two rounds of purification. Samples were run on a MiSeq with a paired-end protocol and read lengths of 150 bp.

For RNA sequencing of *C. albicans* grown in mucin glycans, Illumina RNA-seq was used. Libraries were produced using the KAPA RNA HyperPrep kit (Kapa Biosystems) and sequenced using the Illumina HiSeq platform with a single-end protocol and read lengths of 40 or 50 nucleotides.

### RT-qPCR analysis

A list of the primers used in this study is provided in Supplementary Table 4. qPCR with reverse transcription (RT-qPCR) was performed using a two-step method. First-strand cDNA was synthesized from total RNA using the ProtoScript IV First Strand cDNA Synthesis kit (NEB). The cDNA was used as template for RT-qPCR using a SYBR PowerUp Master Mix kit (Applied Biosystems by Life Technologies) on a Roche LightCycler 480 real-time PCR system. Primers for RT-qPCR were designed on the basis of the published literature or using the NCBI Primer-BLAST tool (<https://www.ncbi.nlm.nih.gov/libproxy.mit.edu/tools/primer-blast/>). The *ACT1* and *18S* rRNA genes were used as endogenous controls as specified. The elimination of contaminating DNA was confirmed using qPCR amplification of *ACT1* and *18S* rRNA genes on control samples that did not have reverse transcriptase added during cDNA synthesis. Changes in gene expression were calculated based on mean change in qPCR cycle threshold ( $C_t$ ) using the  $C_t$  method (fold change =  $2^{-(C_t - C_t)}$ ).

## Analysis of RNA sequencing data

For mucins RNA sequencing experiments, reads were mapped to the *C. albicans* SC5314 haplotype A genome, version A22-s05-m05-r03, retrieved from the *Candida* Genome Database ([www.candidagenome.org](http://www.candidagenome.org)) using Rsubread v1.28.1<sup>53</sup>. Read summarization was performed on the gene level using featureCounts<sup>54</sup> using annotations from a modified version of *C. albicans* SC5314 haplotype A, which only contained protein coding genes. Multimapping read pairs, read pairs mapping across more than one gene, and read pairs in which ends mapped to different chromosomes were removed from downstream analyses. Genes that had <10 counts per million in at least two samples were discarded. Remaining gene counts were normalized using trimmed mean of M-values<sup>55</sup>. Differential expression analysis was performed using limma v3.34.9<sup>56</sup> with voom-transformed read counts<sup>57</sup>. Genes were considered differentially expressed when  $P < 0.05$  after the false-discovery rate was controlled using Benjamini–Hochberg correction.

For mucin glycans RNA sequencing experiments, reads were mapped to the *C. albicans* SC5314 haplotype A genome, version A22-s05-m05-r03, retrieved from the *Candida* Genome Database ([www.candidagenome.org](http://www.candidagenome.org)) using the Galaxy Server<sup>58</sup>. Read summarization was performed on the gene level with annotations from a modified version of *C. albicans* SC5314 haplotype A. Multimapping read pairs, read pairs mapping across more than one gene, and read pairs in which ends mapped to different chromosomes were removed from downstream analyses. Differential expression analysis was performed using DESEQ2<sup>59</sup>. Genes were considered differentially expressed when  $P < 0.05$  after the false-discovery rate was controlled using Benjamini–Hochberg correction.

Functional category (pathway) assignments were obtained from *Candida* Genome Database Gene Ontology annotations and assessed using PANTHER<sup>60</sup>. Over-representation of biological pathways in mucin was assessed using one-sided Fisher's exact test followed by a Benjamini-Hochberg procedure for multiple corrections, for differentially expressed genes from  $n=3$  replicates. Enrichment of pathways in MUC5AC glycans was determined based on mean  $\log_2$ -transformed fold changes from  $n=3$  replicates and calculated with the two-sided Mann-Whitney  $U$ -test followed by a Benjamini-Hochberg procedure for multiple corrections. Heat maps and scatter plots of gene expression data were constructed using GraphPad Prism.

## Murine Wound *C. albicans* Protocol

Female, 8-week old, SKH-1 mice were anesthetized with isoflurane and given buprenorphine (0.05mg/kg) before wounding with a 6-mm punch biopsy to generate two identical full-thickness dermal wounds on the dorsal side of the mouse. Wounds were kept covered with an occlusive dressing (Opsite Flexifix) throughout the duration of the experiment. After a 24 h recovery period, wounds were inoculated with 30  $\mu$ l volume of PBS containing  $10^8$  SC513 Eno1-mCherry yeast. Topical treatments of 30  $\mu$ l of 0.5% MUC2, or PBS were administered to each wound on Day 1, 3, and 5 post-infection. Wounds were gently washed with 500  $\mu$ l of sterile PBS and bandages changed prior to each treatment. Wound fluorescence was imaged daily with IVIS Lumina II optical imaging system to assess

fungal burden. At Day 5 and Day 7, wound biopsy specimens were collected and CFUs were calculated per gram of tissue.

The mice used in this experiment were housed at 72°F at 30% humidity with a 12-hour light/dark cycle. All care of laboratory animals was in accordance with institutional guidelines and approved by the Ohio State University Institutional Animal Care and Use Committee (IACUC) under 2017A00000033-R1.

### Polystyrene attachment assay

Strain HGFP3 was pregrown overnight in YPD medium at 30 °C, diluted to OD<sub>600</sub>=0.1, added into prewarmed RPMI medium in a polystyrene 96-well plate, and incubated at 37 °C for the time indicated in the figure legend. Medium was decanted and plates were washed three times with phosphate-buffered saline. Images were acquired with a confocal laser scanning microscope (LSM 800, Zeiss) equipped with a ×20/1.4 NA objective. The excitation wavelength for GFP was 488 nm. Four images were recorded for each well and for at least three independent wells. Images were analyzed in Fiji as follows: each image was converted to 8-bit and the contrast was enhanced (0.4% saturated pixels), then thresholded to create a binary image. Each image was analyzed using the Analyze Particles tool to measure the surface area covered by cells as described previously<sup>10</sup>. The mean surface area measurements of the images for each condition were calculated.

### Biofilm formation assays and visualization

*In vitro* biofilm growth assays were carried out in RPMI medium by growing the biofilm directly on a 96-well polystyrene plate. Briefly, strain SC5314 was grown overnight in YPD at 30 °C, washed twice with phosphate-buffered saline, then diluted to OD<sub>600</sub>=0.5 in 100 μL of RPMI in a 96-well polystyrene plate. The inoculated plate was incubated at 37 °C for 90 min to facilitate attachment of yeast cells to the surface. Nonadherent cells were washed twice with phosphate-buffered saline, and samples were subsequently submerged in fresh RPMI. Biofilms were grown for 24 h at 37 °C. For CFU enumeration, the medium containing the planktonic cells was removed and plated on YPD plates. Biofilms were resuspended with phosphate-buffered saline, disrupted by pipetting, serially diluted in phosphate-buffered saline, and plated on YPD plates. Biofilms and planktonic cells were imaged using a Zeiss wide-field fluorescence microscope.

### Coculture viability assays

An overnight SC5314 culture grown in YPD was diluted 1:100 into RPMI in a 96-well plate (Mattek) with or without 0.1% MUC5AC glycans and grown for 4 h with shaking at 37 °C. A control well without *C. albicans* was included. Concurrently, 2 mL of LB were inoculated with 40 μL *Pseudomonas aeruginosa* strain PA14 and grown for 4 h with shaking at 37 °C. RPMI was then removed from *C. albicans* and replaced with 200 μL SLB. *P. aeruginosa* was added to a final OD<sub>600</sub>=0.25. At 0 h, 24 h, 48 h, and 72 h, the contents of the wells were homogenized and a 5-μL aliquot was serially diluted in phosphate-buffered saline. Dilutions were plated on YPD agar + Gm<sup>30</sup> + Tet<sup>60</sup> (to select for *C. albicans*) and Cetrimide agar (to select for *P. aeruginosa*) and incubated overnight at 30 °C and 37 °C, respectively. Colonies were counted after incubation.

### Confocal imaging of coculture

Images were acquired with a confocal laser scanning microscope (LSM 800; Zeiss) equipped with a  $\times 63/1.4$  NA oil-immersion objective. Images were analyzed using Zeiss ZEN v.2.1. *C. albicans* was stained with 20  $\mu\text{g}/\text{mL}$  calcofluor white. The excitation and emission wavelengths for calcofluor white were 365 nm and 445 nm, respectively; the excitation and emission wavelengths for mCherry were 587 nm and 610 nm, respectively.

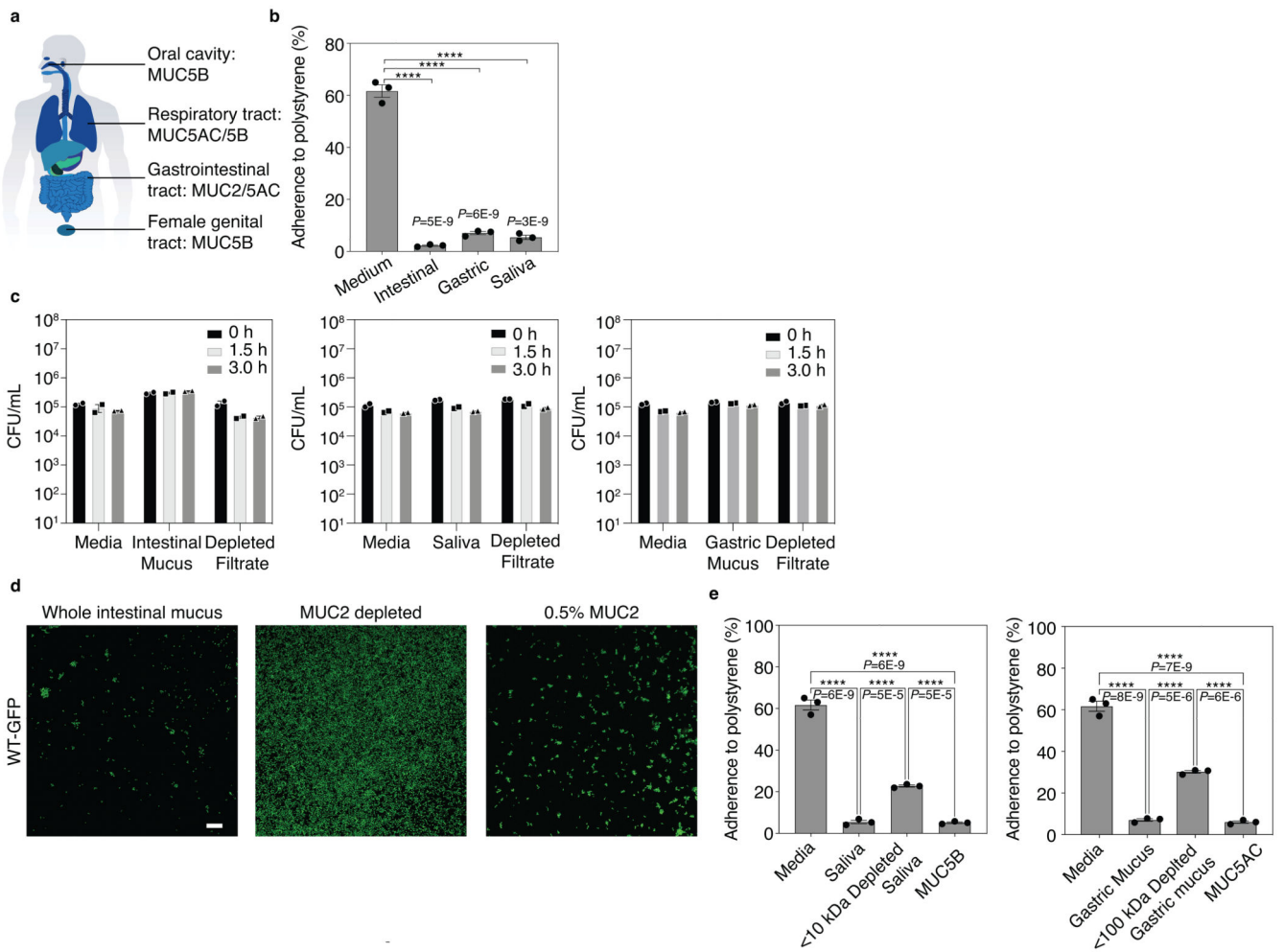
### Glycan synthesis and analysis

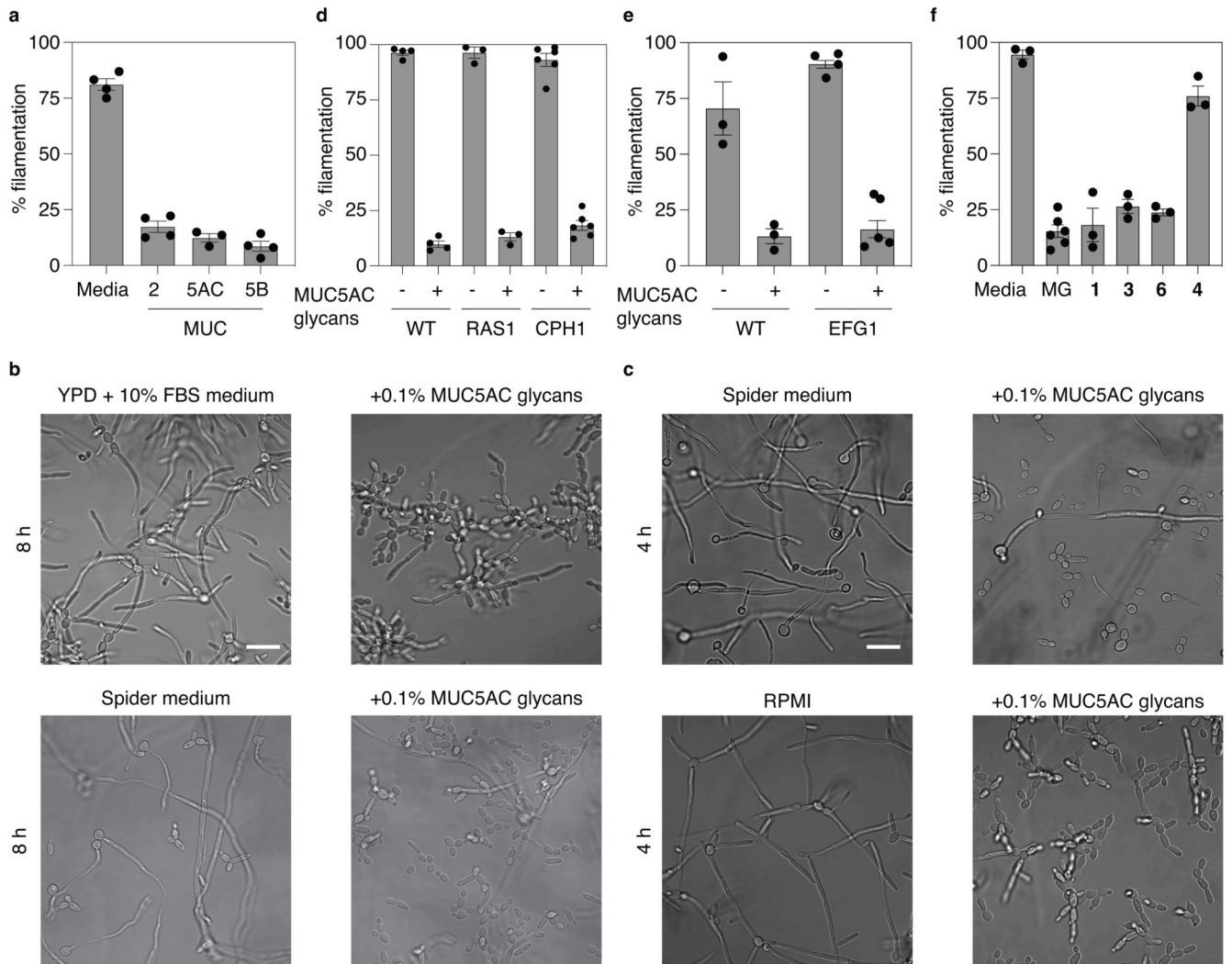
All commercial reagents were used as supplied unless otherwise stated, and solvents were dried and distilled using standard techniques. Thin layer chromatography was performed on silica-coated glass plates (TLC Silica Gel 60 F<sub>254</sub>, Merck) with detection via fluorescence, charring with 5% H<sub>2</sub>SO<sub>4(aq)</sub>, or staining with a ceric ammonium molybdate solution. Organic solutions were concentrated and/or evaporated to dry under vacuum in a water bath (<50 °C). Molecular sieves were dried at 400 °C under vacuum for 20-30 min prior to use. Amberlite IR-120H resin was washed extensively with MeOH and dried under vacuum prior to use. Medium-pressure liquid chromatography was performed using a CombiFlash Companion equipped with RediSep normal-phase flash columns, and solvent gradients refer to sloped gradients with concentrations reported as % v/v. Nuclear magnetic resonance spectra were recorded on a Bruker Avance DMX-500 (500 MHz) spectrometer, and assignments achieved with the assistance of 2D gCOSY, 2D gTOCSY, 2D gHSQC, and 2D gHMBC; chemical shifts are expressed in ppm and referenced to either Si(CH<sub>3</sub>)<sub>4</sub> (for CDCl<sub>3</sub>), residual CHD<sub>2</sub>OD (for CD<sub>3</sub>OD), or a MeOH internal standard (for D<sub>2</sub>O). Low-resolution electron-spray ionization mass spectrometry was performed with a Waters micromass ZQ. High-resolution mass spectrometry was performed with an Agilent 1100 LC equipped with a photodiode array detector, and a Micromass QTOF I equipped with a 4 GHz digital-time converter. Optical rotation was determined in a 10-cm cell at 20 °C using a Perkin-Elmer Model 341 polarimeter. High-performance liquid chromatography was performed with an Agilent 1100 LC equipped with an Atlantis T3 (3 mm, 2.1x100 mm) C18 column and ELSD detection.

### Statistical analysis

Unless noted otherwise, experiments were performed with at least three biological replicates consisting of at least three technical replicates, and results are presented as mean  $\pm$  SEM. Microscopy images depicted are representative and similar results were observed in different fields of view across at minimum three independent biological replicates. Raw data are available as Source Data. MUC2, MUC5AC, and MUC5B and their associated glycans were tested from several purification batches with consistent results.

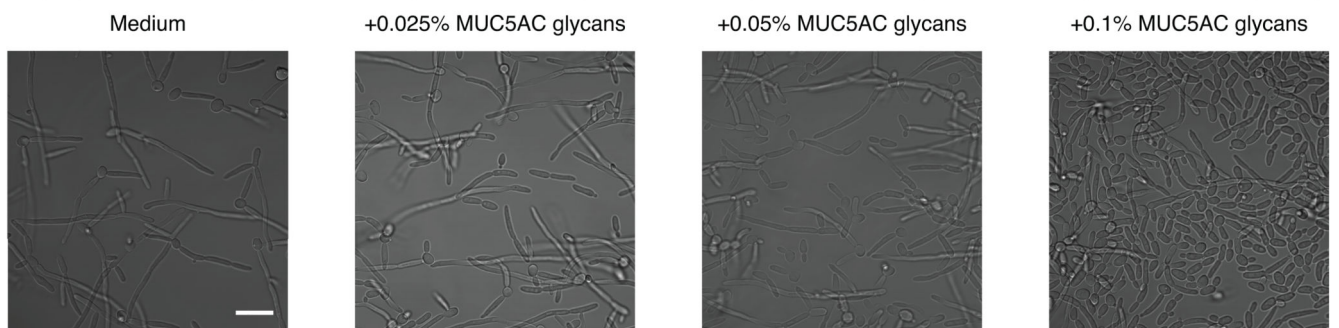
## Extended Data



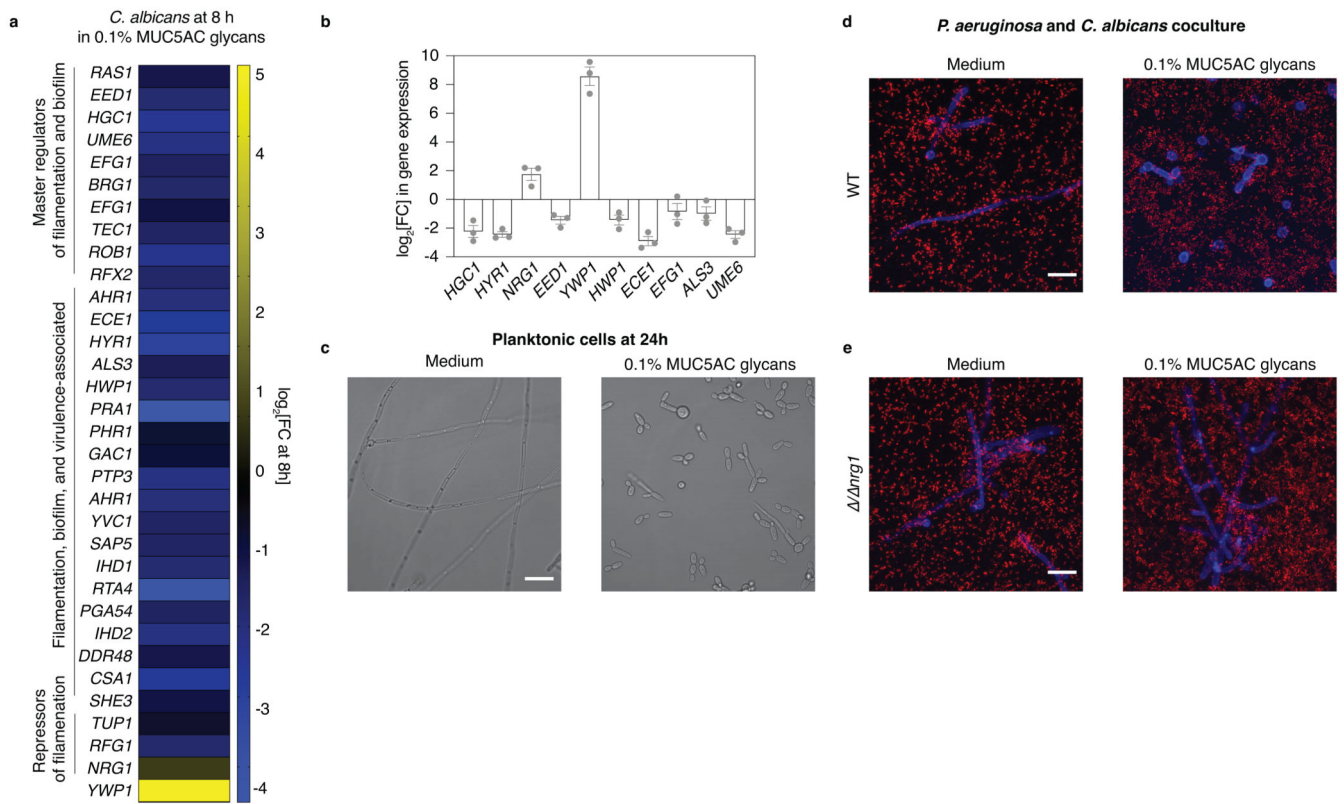


Extended Data Figure 2.

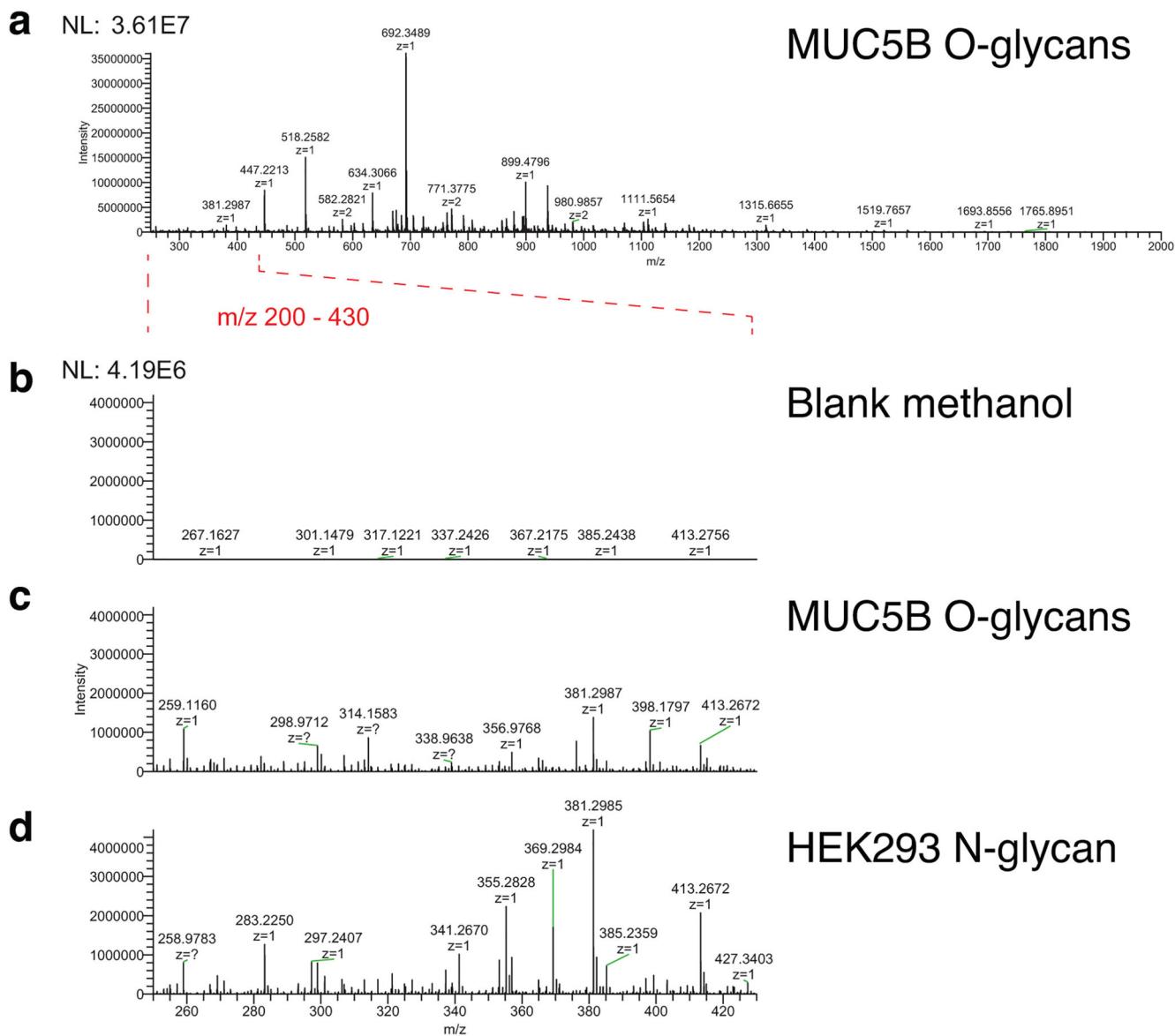
Filamentation assay in the presence of:



Extended Data Figure 3.



Extended Data Figure 4.



Extended Data Figure 5.

## Supplementary Material

Refer to Web version on PubMed Central for supplementary material.

## Acknowledgments

The authors thank B. Wang and V.P. Patil for comments on the manuscript. This research was supported by The NIH NIBIB award R01EB017755-04 (OSP 6940725) (to K.R.), the MRSEC Program of the National Science Foundation under award DMR-1419807 (to K.R.), the National Science Foundation Career award PHY1454673 (to K.R.), the U.S. Army Research Office under cooperative agreement W911NF-19-2-0026 for the Institute for Collaborative Biotechnologies (to K.R.), the core center grant P30-ES002109 from the National Institute of Environmental Health Sciences P30-ES002109 (to K.R.), the Toxicology Training Grant support T32-ES007020 (to J.T), the National Center for Functional Glycomics Grant P41GM103694 (to R.D.C.), the Swiss National Science Spark Grant Foundation CRSK-3\_196773 (to R.H), and the NIH NIGMS award R35GM124594 (to C.J.N.), by the

Kamangar family in the form of an endowed chair (to C.J.N.). The content is the sole responsibility of the authors and does not represent the views of the funders. The funders had no role in the design of the study; in the collection, analyses, or interpretation of data; in the writing of the manuscript; or in the decision to publish the results.

## Data and materials availability

High-throughput sequencing data presented are deposited in the Gene Expression Omnibus (GEO) under accession number GSE197249 (Fig. 1) and GSE192826 (Fig. 2,3). All raw mass spectrometric data related to mucin glycan profiles were deposited at GlycoPost, Accession #GPST000254 for non-sulfated glycans and Accession #GPST000258 for sulfated glycans. Source data are provided with this paper. All other data are available from the corresponding author upon reasonable request.

## References

1. Ganguly S, Mitchell AP. Mucosal biofilms of *Candida albicans*. *Curr Opin Microbiol*. 2011; 14: 380–385. [PubMed: 21741878]
2. Valle Arevalo A, Nobile CJ. Interactions of microorganisms with host mucins: a focus on *Candida albicans*. *FEMS microbiology reviews*. 2020; 44: 645–654. [PubMed: 32627827]
3. Pappas PG, Lionakis MS, Arendrup MC, Ostrosky-Zeichner L, Kullberg BJ. Invasive candidiasis. *Nat Rev Dis Primers*. 2018; 4: 1–20. [PubMed: 29930242]
4. Perlin DS. Antifungals: From Genomics to Resistance and the Development of Novel Agents. *Clinical Infectious Diseases*. 2015; 61: 1213–1214.
5. Calderone RA, Fonzi WA. Virulence factors of *Candida albicans*. *Trends in Microbiology*. 2001; 9: 327–335. [PubMed: 11435107]
6. Nobile CJ, Johnson AD. *Candida albicans* Biofilms and Human Disease. *Annu Rev Microbiol*. 2015; 69: 71–92. [PubMed: 26488273]
7. Kennedy MJ, Volz PA. Ecology of *Candida albicans* gut colonization: inhibition of *Candida* adhesion, colonization, and dissemination from the gastrointestinal tract by bacterial antagonism. *Infect Immun*. 1985; 49: 654–663. [PubMed: 3897061]
8. Corfield AP. Mucins: A biologically relevant glycan barrier in mucosal protection. *Biochimica et Biophysica Acta (BBA) - General Subjects*. 2015; 1850: 236–252. [PubMed: 24821013]
9. Wang BX, Wu CM, Ribbeck K. Home, sweet home: how mucus accommodates our microbiota. *The FEBS Journal*. 2021; 288: 1789–1799. [PubMed: 32755014]
10. Kavanaugh NL, Zhang AQ, Nobile CJ, Johnson AD, Ribbeck K. Mucins Suppress Virulence Traits of *Candida albicans*. *mBio*. 2014; 5 e01911-14 [PubMed: 25389175]
11. Turner BS, Bhaskar KR, Hadzopoulou-Cladaras M, LaMont JT. Cysteine-rich regions of pig gastric mucin contain von Willebrand factor and cystine knot domains at the carboxyl terminal. *Biochimica et Biophysica Acta (BBA) - Gene Structure and Expression*. 1999; 1447: 77–92. [PubMed: 10500247]
12. Krupa L, et al. Comparing the permeability of human and porcine small intestinal mucus for particle transport studies. *Sci Rep*. 2020; 10 20290 [PubMed: 33219331]
13. Celli J, et al. Viscoelastic Properties and Dynamics of Porcine Gastric Mucin. *Biomacromolecules*. 2005; 6: 1329–1333. [PubMed: 15877349]
14. Han T-L, Cannon RD, Villas-Bôas SG. The metabolic basis of *Candida albicans* morphogenesis and quorum sensing. *Fungal Genetics and Biology*. 2011; 48: 747–763. [PubMed: 21513811]
15. Tailford LE, Crost EH, Kavanaugh D, Juge N. Mucin glycan foraging in the human gut microbiome. *Front Genet*. 2015; 6
16. Lindén SK, et al. MUC1 limits *Helicobacter pylori* infection both by steric hindrance and by acting as a releasable decoy. *PLoS Pathog*. 2009; 5 e1000617 [PubMed: 19816567]
17. Chatterjee M, et al. Understanding the adhesion mechanism of a mucin binding domain from *Lactobacillus fermentum* and its role in enteropathogen exclusion. *International Journal of Biological Macromolecules*. 2018; 110: 598–607. [PubMed: 29061520]

18. Wheeler KM, et al. Mucin glycans attenuate the virulence of *Pseudomonas aeruginosa* in infection. *Nature Microbiology*. 2019; 4: 2146–2154.
19. Bergstrom KSB, Xia L. Mucin-type O-glycans and their roles in intestinal homeostasis. *Glycobiology*. 2013; 23: 1026–1037. [PubMed: 23752712]
20. Banerjee M, et al. UME6, a Novel Filament-specific Regulator of *Candida albicans* Hyphal Extension and Virulence. *Mol Biol Cell*. 2008; 19: 1354–1365. [PubMed: 18216277]
21. Zheng X, Wang Y, Wang Y. Hgc1, a novel hypha-specific G1 cyclin-related protein regulates *Candida albicans* hyphal morphogenesis. *EMBO J*. 2004; 23: 1845–1856. [PubMed: 15071502]
22. Granger BL, Flenniken ML, Davis DA, Mitchell AP, Cutler JE. Yeast wall protein 1 of *Candida albicans*. *Microbiology (Reading)*. 2005; 151: 1631–1644. [PubMed: 15870471]
23. Sudbery PE. Growth of *Candida albicans* hyphae. *Nature Reviews Microbiology*. 2011; 9: 737–748. [PubMed: 21844880]
24. Lu Y, Su C, Liu H. *Candida albicans* hyphal initiation and elongation. *Trends in Microbiology*. 2014; 22: 707–714. [PubMed: 25262420]
25. Feng Q, Summers E, Guo B, Fink G. Ras signaling is required for serum-induced hyphal differentiation in *Candida albicans*. *J Bacteriol*. 1999; 181: 6339–6346. [PubMed: 10515923]
26. Bockmühl DP, Ernst JF. A Potential Phosphorylation Site for an A-Type Kinase in the Efg1 Regulator Protein Contributes to Hyphal Morphogenesis of *Candida albicans*. *Genetics*. 2001; 157: 1523–1530. [PubMed: 11290709]
27. Leuker CE, Sonneborn A, Delbrück S, Ernst JF. Sequence and promoter regulation of the PCK1 gene encoding phosphoenolpyruvate carboxykinase of the fungal pathogen *Candida albicans*. *Gene*. 1997; 192: 235–240. [PubMed: 9224895]
28. Shapiro RS, Robbins N, Cowen LE. Regulatory Circuitry Governing Fungal Development, Drug Resistance, and Disease. *Microbiol Mol Biol Rev*. 2011; 75: 213–267. [PubMed: 21646428]
29. Nobile CJ, et al. A Recently Evolved Transcriptional Network Controls Biofilm Development in *Candida albicans*. *Cell*. 2012; 148: 126–138. [PubMed: 22265407]
30. Lohse MB, Gulati M, Johnson AD, Nobile CJ. Development and regulation of single- and multi-species *Candida albicans* biofilms. *Nature Reviews Microbiology*. 2018; 16: 19–31. [PubMed: 29062072]
31. Morales DK, Hogan DA. *Candida albicans* interactions with bacteria in the context of human health and disease. *PLoS Pathog*. 2010; 6 e1000886 [PubMed: 20442787]
32. Hogan DA, Kolter R. *Pseudomonas-Candida* Interactions: An Ecological Role for Virulence Factors. *Science*. 2002; 296: 2229–2232. [PubMed: 12077418]
33. Brand A, Barnes JD, Mackenzie KS, Odds FC, Gow NAR. Cell wall glycans and soluble factors determine the interactions between the hyphae of *Candida albicans* and *Pseudomonas aeruginosa*. *FEMS Microbiol Lett*. 2008; 287: 48–55. [PubMed: 18680523]
34. Jin C, et al. Structural Diversity of Human Gastric Mucin Glycans. *Mol Cell Proteomics*. 2017; 16: 743–758. [PubMed: 28461410]
35. Amon R, Reuven EM, Leviatan Ben-Arye S, Padler-Karavani V. Glycans in immune recognition and response. *Carbohydr Res*. 2014; 389: 115–122. [PubMed: 24680512]
36. Cummings RD, Pierce JM. The Challenge and Promise of Glycomics. *Chemistry & Biology*. 2014; 21: 1–15. [PubMed: 24439204]
37. Dube DH, Bertozzi CR. Glycans in cancer and inflammation — potential for therapeutics and diagnostics. *Nat Rev Drug Discov*. 2005; 4: 477–488. [PubMed: 15931257]
38. Hevey R. Strategies for the Development of Glycomimetic Drug Candidates. *Pharmaceuticals*. 2019; 12: 55.
39. Hevey R. Bioisosteres of Carbohydrate Functional Groups in Glycomimetic Design. *Biomimetics*. 2019; 4: 53.
40. Brockhausen I. Mucin-type O-glycans in human colon and breast cancer: glycodynamics and functions. *EMBO reports*. 2006; 7: 599–604. [PubMed: 16741504]
41. Tabak LA. The role of mucin-type O-glycans in eukaryotic development. *Seminars in Cell & Developmental Biology*. 2010; 21: 616–621. [PubMed: 20144722]

42. Kudelka MR, Ju T, Heimburg-Molinaro J, Cummings RD. Simple Sugars to Complex Disease—Mucin-Type O-Glycans in Cancer. *Adv Cancer Res.* 2015; 126: 53–135. [PubMed: 25727146]
43. Giancchetti E, Arena A, Fierabracci A. Sialic Acid-Siglec Axis in Human Immune Regulation, Involvement in Autoimmunity and Cancer and Potential Therapeutic Treatments. *IJMS.* 2021; 22: 5774 [PubMed: 34071314]
44. Donohue DS, Ielasi FS, Goossens KVY, Willaert RG. The N-terminal part of Als1 protein from *Candida albicans* specifically binds fucose-containing glycans. *Molecular Microbiology.* 2011; 80: 1667–1679. [PubMed: 21585565]
45. Lee KL, Buckley HR, Campbell CC. An amino acid liquid synthetic medium for the development of mycelial and yeast forms of *Candida Albicans*. *Sabouraudia.* 1975; 13: 148–153. [PubMed: 808868]
46. Wagner CE, Turner BS, Rubinstein M, McKinley GH, Ribbeck K. A rheological study of the association and dynamics of MUC5AC gels. *Biomacromolecules.* 2017; 18: 3654–3664. [PubMed: 28903557]
47. Lieleg O, Lieleg C, Bloom J, Buck CB, Ribbeck K. Mucin biopolymers as broad-spectrum antiviral agents. *Biomacromolecules.* 2012; 13: 1724–1732. [PubMed: 22475261]
48. Huang Y, Mechref Y, Novotn MV. Microscale nonreductive release of O-linked glycans for subsequent analysis through MALDI mass spectrometry and capillary electrophoresis. *Anal Chem.* 2001; 73: 6063–6069. [PubMed: 11791581]
49. Aoki K, et al. Dynamic developmental elaboration of N-linked glycan complexity in the *Drosophila melanogaster* embryo. *J Biol Chem.* 2007; 282: 9127–9142. [PubMed: 17264077]
50. Liu Y, et al. The minimum information required for a glycomics experiment (MIRAGE) project: improving the standards for reporting glycan microarray-based data. *Glycobiology.* 2017; 27: 280–284. [PubMed: 27993942]
51. Mehta AY, Cummings RD. GlycoGlyph: a glycan visualizing, drawing and naming application. *Bioinformatics.* 2020; 36: 3613–3614. [PubMed: 32170934]
52. Watanabe Y, Aoki-Kinoshita KF, Ishihama Y, Okuda S. GlycoPOST realizes FAIR principles for glycomics mass spectrometry data. *Nucleic Acids Res.* 2021; 49: D1523–D1528. [PubMed: 33174597]
53. Liao Y, Smyth GK, Shi W. The Subread aligner: fast, accurate and scalable read mapping by seed-and-vote. *Nucleic Acids Research.* 2013; 41: e108. [PubMed: 23558742]
54. Liao Y, Smyth GK, Shi W. featureCounts: an efficient general purpose program for assigning sequence reads to genomic features. *Bioinformatics.* 2014; 30: 923–930. [PubMed: 24227677]
55. Robinson MD, Oshlack A. A scaling normalization method for differential expression analysis of RNA-seq data. *Genome Biology.* 2010; 11: R25. [PubMed: 20196867]
56. Ritchie ME, et al. limma powers differential expression analyses for RNA-sequencing and microarray studies. *Nucleic Acids Research.* 2015; 43: e47. [PubMed: 25605792]
57. Law CW, Chen Y, Shi W, Smyth GK. voom: precision weights unlock linear model analysis tools for RNA-seq read counts. *Genome Biology.* 2014; 15: R29. [PubMed: 24485249]
58. Afgan E, et al. The Galaxy platform for accessible, reproducible and collaborative biomedical analyses: 2018 update. *Nucleic Acids Res.* 2018; 46: W537–W544. [PubMed: 29790989]
59. Love MI, Huber W, Anders S. Moderated estimation of fold change and dispersion for RNA-seq data with DESeq2. *Genome Biol.* 2014; 15: 550. [PubMed: 25516281]
60. Mi H, et al. Protocol Update for large-scale genome and gene function analysis with the PANTHER classification system (v.14.0). *Nature Protocols.* 2019; 14: 703–721. [PubMed: 30804569]

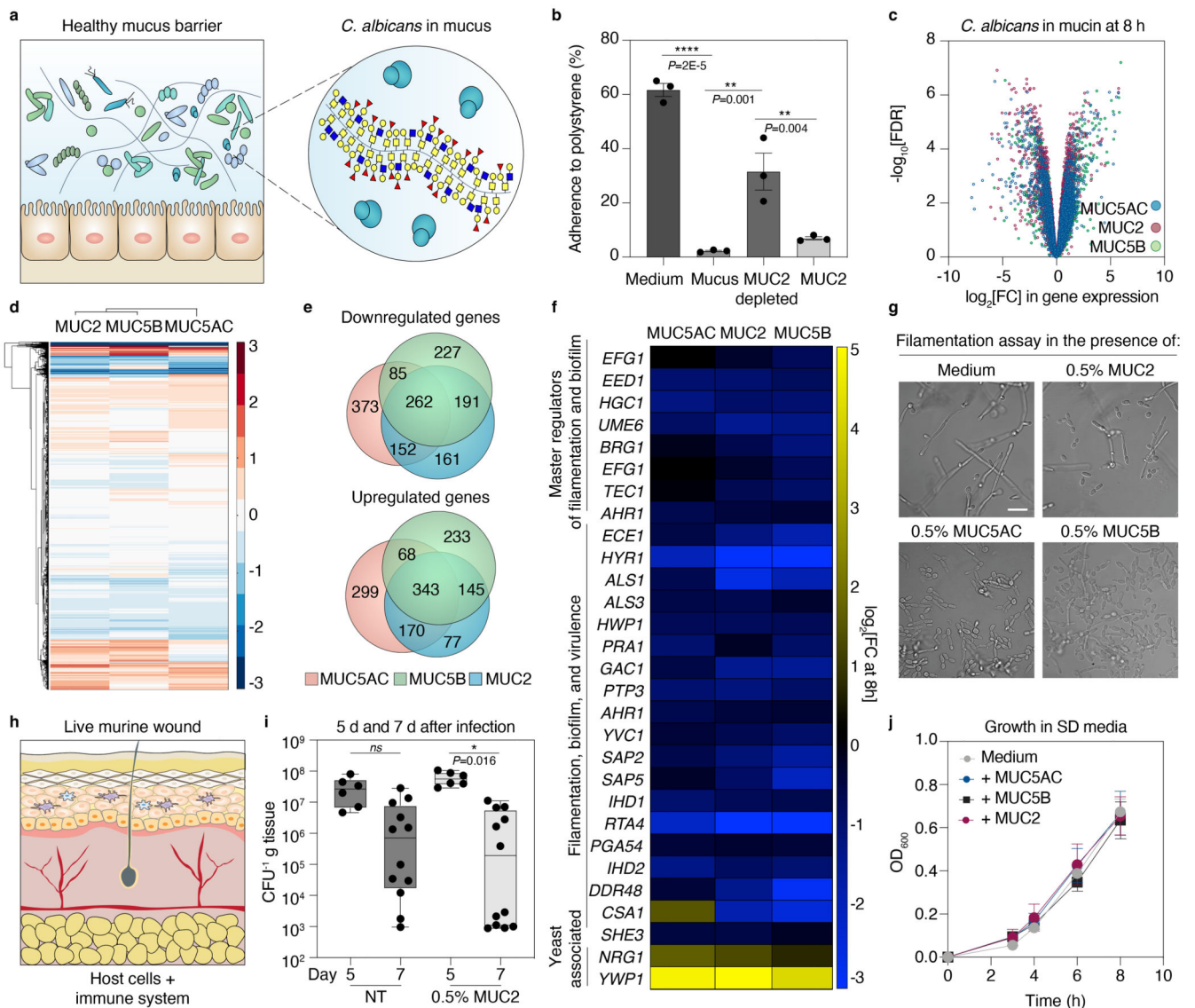


**Figure 1. Mucins across major mucosal surfaces share a conserved function in attenuating *C. albicans* virulence *in vitro* and *in vivo***

- a) The mucus barrier hosts a diverse range of microorganisms while limiting infections. *Candida albicans*, an opportunistic fungal pathogen, resides within the mucosa.
- b) Native mucus suppresses fungal adherence to polystyrene wells. Depletion of intestinal mucus components increases fungal adherence. Supplementation of mucus filtrates with purified MUC2 reduces adhesion. Bars indicate mean  $\pm$  SEM from  $n=3$  biologically independent replicates using fluorescence images. Significance was assessed using one-way ANOVA followed by Bonferroni multiple comparisons test; \*\*\*\* $P<0.0001$  \*\* $P<0.01$ .
- c) MUC5AC, MUC5B, and MUC2 elicit global transcriptional responses in *C. albicans*.
- d) Dendrogram and hierarchical clustering heat map of genome-wide expression profiles from MUC5AC, MUC2, and MUC5B. Clustering was performed first along the sample dimension and then along the individual gene dimension using the Matlab clustergram

function with Euclidean distances and Ward's linkage method. Color scale bar units are in SDs.

e) Venn diagrams indicate the number of genes differentially expressed after exposure to mucins.

f) RNA sequencing data for selected genes belonging to filamentation, biofilm formation, and pathogenesis.

g) Mucins across three mucosal surfaces suppress filamentation. Phase-contrast images of SC5314 cells grown in RPMI medium with or without mucins at 37 °C for 8 h. Scale bar, 20 μm.

h) Fungal viability was monitored in a live dermal wound model.

i) Fungal burden on murine puncture wounds at 5 and 7 d after treatment with MUC2 or a mock-treatment (NT) control. Symbols represent colony-forming units from  $n=6$  biologically independent replicates. The center bars indicate the median, the box limits indicate the upper and lower quartiles, and the whiskers indicate the minimum and maximum values. Significance was assessed using Welch and Brown-Forsythe ANOVA (assumes unequal variance) followed by Dunnett T3 multiple comparisons test;  $*P=0.016$ .

j) Growth is not altered by mucins in the synthetic defined medium (SD). Data are the mean OD<sub>600</sub> measurements ± SEM;  $n=4$  (MUC5B, MUC5AC),  $n=6$  (Medium, MUC2) biologically independent replicates.

For **c,d,e,f**, a complete list of FC values and FDR-adjusted  $P$  values is provided in Supplementary Data 1.  $P$  values were determined using a two-tailed moderated  $t$ -test and FDR-adjusted ( $P<0.05$ ) using Benjamini–Hochberg correction for multiple comparisons. Data from  $n=3$  biologically independent replicates.

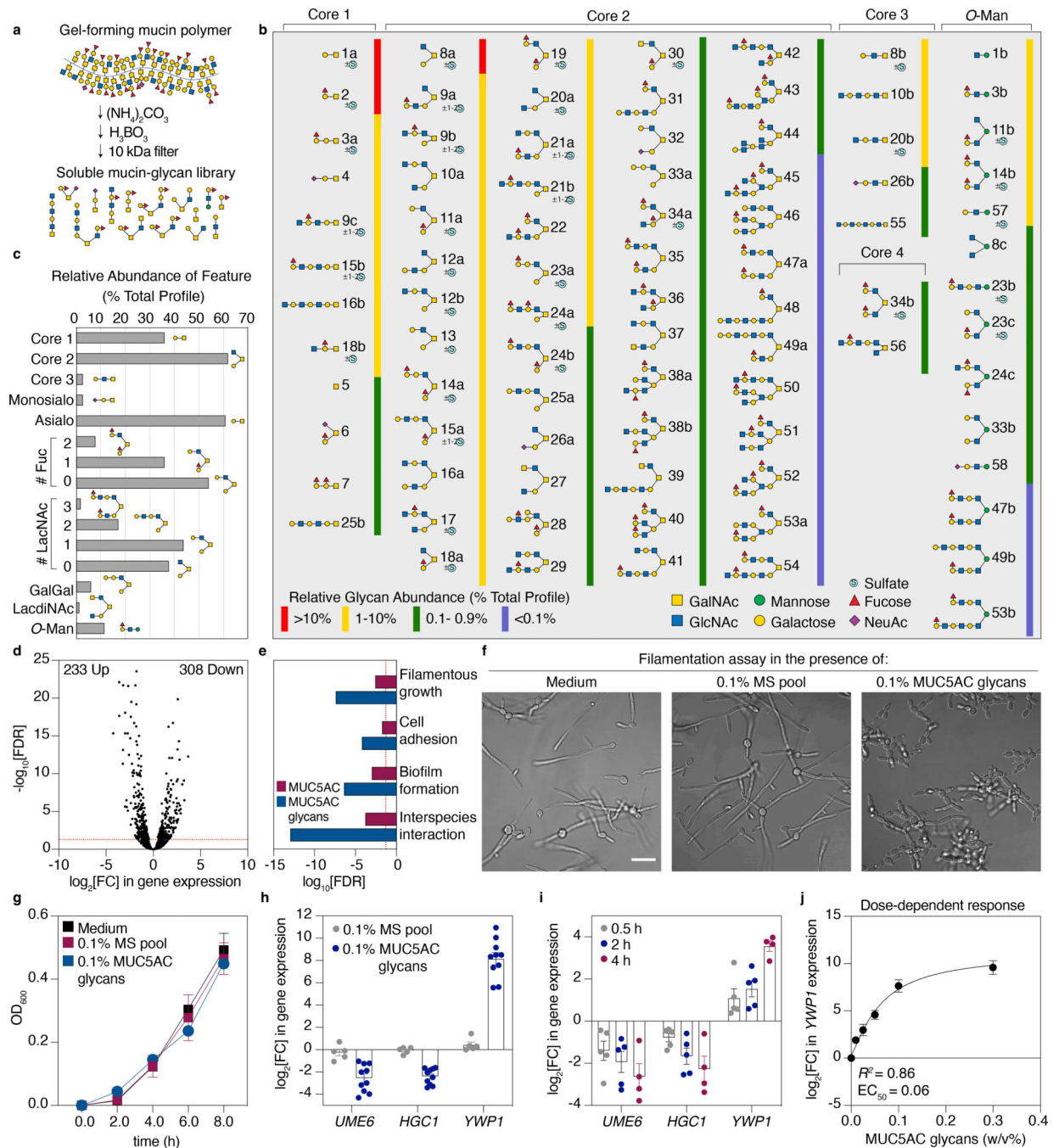


**Figure 2. Mucin glycans potentially inhibit filamentation in a time- and dose-dependent manner**

a) Mucin glycans were isolated (Methods) from the protein backbone using alkaline  $\beta$ -elimination.

b) Structural diversity and relative abundances of MUC5AC glycans analyzed by NSI-MS (Methods). The complete list of structures is listed in Supplementary Table 1. Negative mode NSI-MS detected sulfation on a subset of O-glycans, indicated with the letter S in a cyan circle (Supplementary Table 2). NeuAc, N-acetylneuraminic acid.

- c) Relative abundances of glycan features in the MUC5AC glycan pool. LacNAc, *N*-acetylglucosamine or Gal $\beta$ 1-3/4GlcNAc; GalGal, Gal $\alpha$ 1-3Gal; LacdiNAc, GalNAc $\beta$ 1-4GlcNAc; O-Man, mannose linked  $\alpha$ 1 to serine or threonine.
- d) MUC5AC glycans elicit global transcriptional responses in *C. albicans*.
- e) Functional enrichment analyses reveal key virulence pathways among downregulated genes. Significance of enrichment was calculated using a two-tailed Mann-Whitney *U* test based on mean log<sub>2</sub>-transformed FCs from *n*=3 biologically independent replicates. The dotted line represents the threshold for significance (FDR-adjusted *P*<0.05).
- f) MUC5AC glycans inhibit filamentation. Phase-contrast images of WT SC5314 cells grown in RPMI medium alone, the monosaccharide (MS) pool or mucin glycans at 37 °C for 8 h. Scale bar, 20  $\mu$ m.
- g) Growth is not altered in the presence of the MS pool or mucin glycans in synthetic defined medium. Data are mean OD<sub>600</sub> measurements  $\pm$  SEM from *n*=3 biologically independent replicates.
- h) Mucin glycans, unlike their monosaccharide components, downregulate signature virulence genes. Bars indicate mean  $\pm$  SEM from *n*=5 (MS pool), *n*=10 (MUC5AC glycans) biologically independent replicates.
- i) MUC5AC glycans downregulate virulence gene expression over a prolonged time course. Bars indicate mean  $\pm$  SEM from *n*=5 (0.5 h, 2 h), *n*=4 (4 h) biologically independent replicates.
- j) Mucin glycans regulate *YWPI* expression in a concentration-dependent manner. Data points indicate mean  $\pm$  SEM and are fitted to a nonlinear agonist binding curve from *n*=3 (0.01%, 0.025%, 0.3%), *n*=5 (0.05%, 0.1%) biologically independent replicates.
- For **d,e**, a complete list of FC values and FDR-adjusted *P*-values is provided in Supplementary Data 3 from *n*=3 biologically independent replicates. *P* values were determined using a two-tailed Wald test and FDR-adjusted (*P*<0.05) using Benjamini–Hochberg correction for multiple comparisons.
- For **h,i,j**, data are log<sub>2</sub>-transformed qPCR measurements normalized to a control gene (*ACT1*).

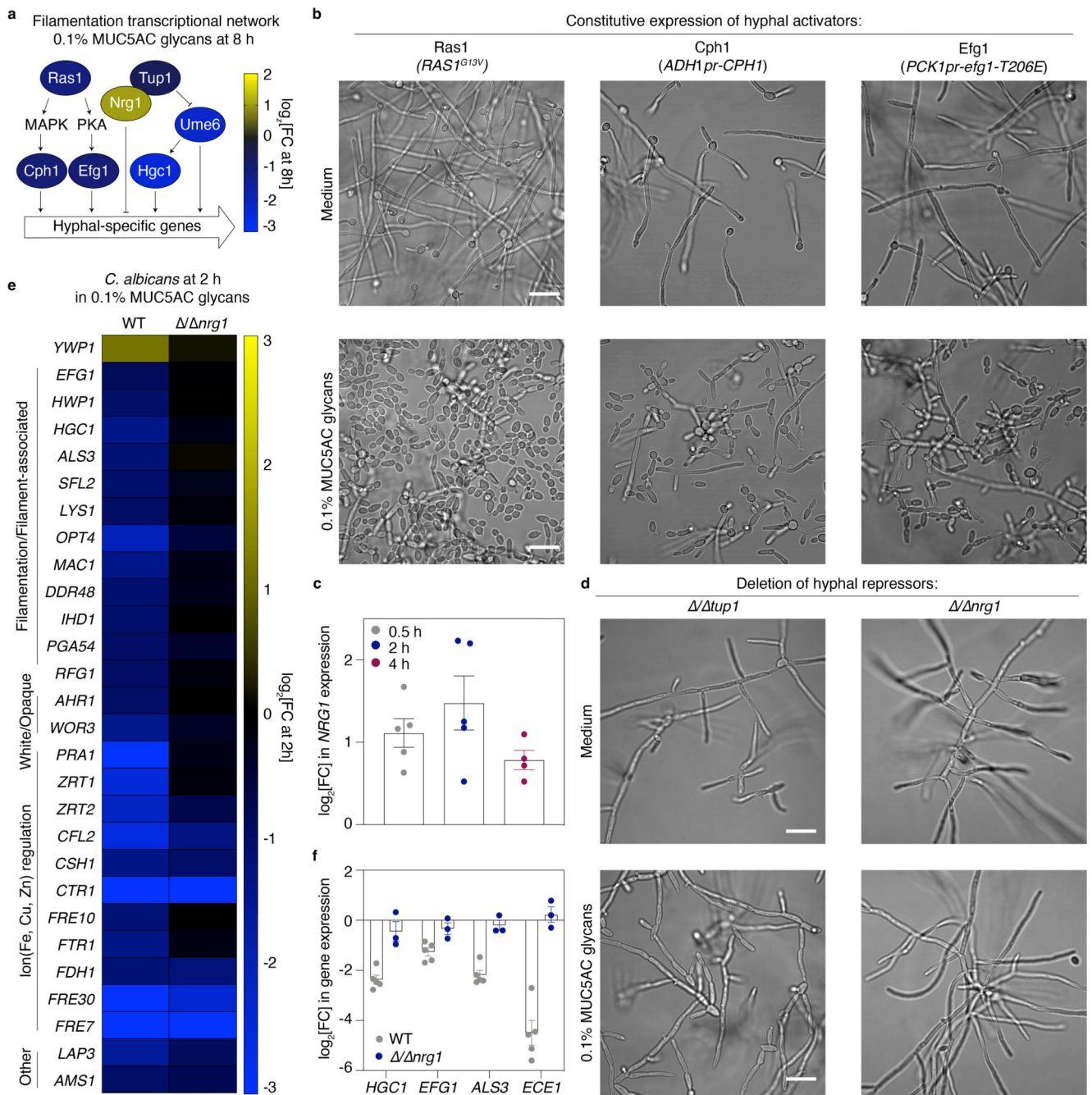


**Figure 3. Mucin glycans act via Nrg1 to prevent filamentation and hyphal gene expression**

a) MUC5AC glycans suppress the expression of key activators of the filamentation pathway.

RNA-seq data for selected genes that are differentially regulated in the presence of MUC5AC glycans from  $n=3$  biologically independent replicates (Supplementary Data 3).  $P$  values were determined using a two-tailed Wald test and FDR-adjusted ( $P<0.05$ ) using Benjamini–Hochberg correction for multiple comparisons.

b) MUC5AC glycans inhibit filamentation in strains hyperactivating the cAMP and MAPK pathways. Phase-contrast images of cells of the indicated genotype were grown in the

presence or absence of MUC5AC glycans in Spider medium (*PCKpr-efg1-T206E*) or RPMI medium (*prADHI-CPH1, RAS1<sup>G13V</sup>*) at 37 °C for 4 h. Scale bar, 20  $\mu$ m.

c) Expression of *NRG1* in wild-type (WT) SC5314 cells after 0.5 h, 2 h, or 4 h in 0.1% MUC5AC glycans (versus growth in medium alone). Gene expression was measured with qRT-PCR and normalized to a control gene (*ACT1*). Bars indicate the mean  $\pm$  SEM from  $n=5$  (0.5 h, 2 h),  $n=4$  (4 h) biologically independent replicates.

d) Loss of *NRG1* or *TUP1* leads to hyperfilamentation in the presence or absence of mucin glycans. Phase-contrast images of cells of the indicated genotype were grown in the presence or absence of MUC5AC glycans in RPMI medium at 37 °C for 4 h. Scale bar, 20  $\mu$ m.

e) FC values for gene-expression changes in WT SC5314 or / *nrg1* mutant cells after 2 h in MUC5AC glycans (versus growth in medium alone). Complete lists of FC values and FDR-adjusted *P* values from  $n=2$  biologically independent replicates are provided in Supplementary Data 5 and 6. *P* values were determined using a two-tailed Wald test and FDR-adjusted ( $P<0.05$ ) using Benjamini–Hochberg correction for multiple comparisons.

f) Expression of filamentation-associated genes in WT SC5314 or / *nrg1* mutant cells after 2 h in MUC5AC glycans (versus growth in medium alone). Gene expression was measured with qRT-PCR and normalized to a control gene (*ACT1*). Bars indicate the mean  $\pm$  SEM from  $n=5$  (WT),  $n=3$  ( *nrg1*) biologically independent replicates.

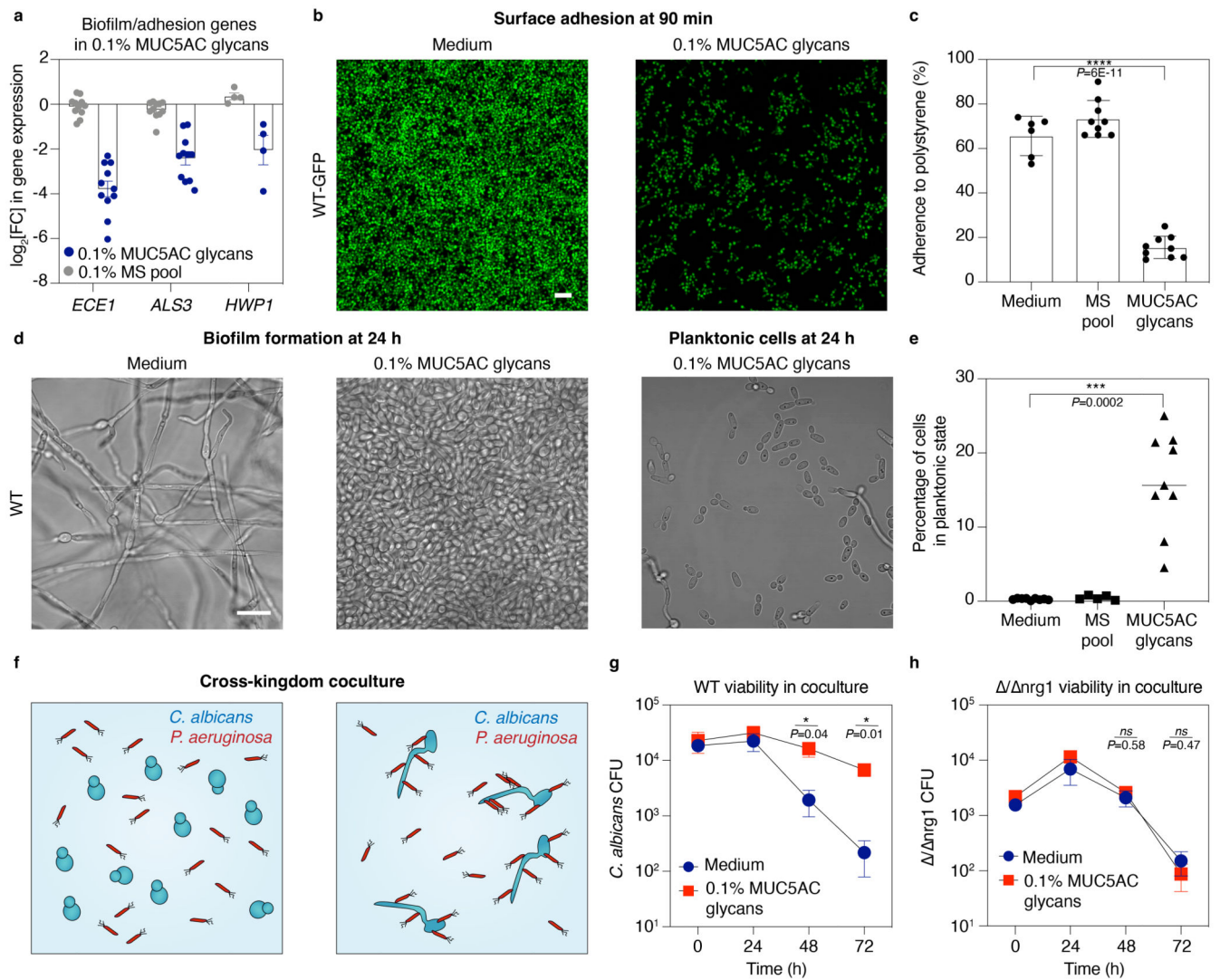


**Figure 4. Mucin glycans downregulate virulence cascades and mediate fungal-bacterial dynamics**

- a) Mucin glycans downregulate the expression of adhesion-related genes. Gene expression was measured by qRT-PCR and normalized to a control gene (*ACT1*). Bars indicate mean  $\pm$  SEM from  $n=11$  (*ECE1*, *ALS3*),  $n=4$  (*HWPI*) biologically independent replicates. MS, monosaccharide.
- b) Fluorescence microscopy images assaying adhesion of wild-type (WT) *C. albicans* expressing green fluorescent protein (GFP) at 90 min in the presence or absence of MUC5AC glycans. Scale bar, 50  $\mu$ m.
- c) Quantification of adhesion to polystyrene wells using fluorescence images from  $n=9$  (MS pool, MUC5AC glycans),  $n=6$  (Medium) biologically independent replicates. Bars indicate mean  $\pm$  SEM. Significance was assessed using ordinary one-way ANOVA followed by Bonferroni multiple comparisons test; \*\*\*\* $P<0.0001$ .
- d) Phase-contrast images of (left, middle) biofilm and (right) planktonic WT cells grown for 24 h in the (left) absence or (middle, right) presence of MUC5AC glycans. Non-adhered

(planktonic) cells in the MUC5AC glycan-exposed biofilms were imaged (right). Scale bar, 20  $\mu\text{m}$ .

e) Quantification of CFUs in the supernatant (planktonic cells) relative to total CFU from adhered cells in the biofilm from  $n=9$  (Medium, MUC5AC glycans) and  $n=5$  (MS pool) biologically independent replicates. Significance was assessed using Brown-Forsythe and Welch ANOVA tests (assumes unequal variance) followed by Dunnett T3 multiple comparisons test; \*\*\* $P=0.0002$ .

f) Schematics of *in vitro* *P. aeruginosa* (bacteria) and *C. albicans* (yeast) interactions. Left: *P. aeruginosa* does not effectively kill yeast form *C. albicans*. Right: In contrast, *P. aeruginosa* adheres to *C. albicans* hyphae and secretes toxins, leading to fungal death.

g) *C. albicans* yeast cells were diluted into RPMI medium with or without MUC5AC glycans for 4 h. *P. aeruginosa* cells ( $\text{OD}_{600}=0.25$ ) in spent LB were added to the *C. albicans* cells with or without MUC5AC glycans and cocultured at 37 °C for 72 h. The fungal viable cell population was determined daily by plating. \* $P=0.04$  (48 h); \* $P=0.014$  (72 h).

h) Cultures of *nrg1* cells were treated as in (g) with or without MUC5AC glycans and cocultured with *P. aeruginosa* at 37 °C for 72 h.

For **g,h**, Data are mean  $\pm$  SEM from  $n=5$  biologically independent replicates. Significance was assessed using two-tailed Student's *t*-tests with Welch's correction.

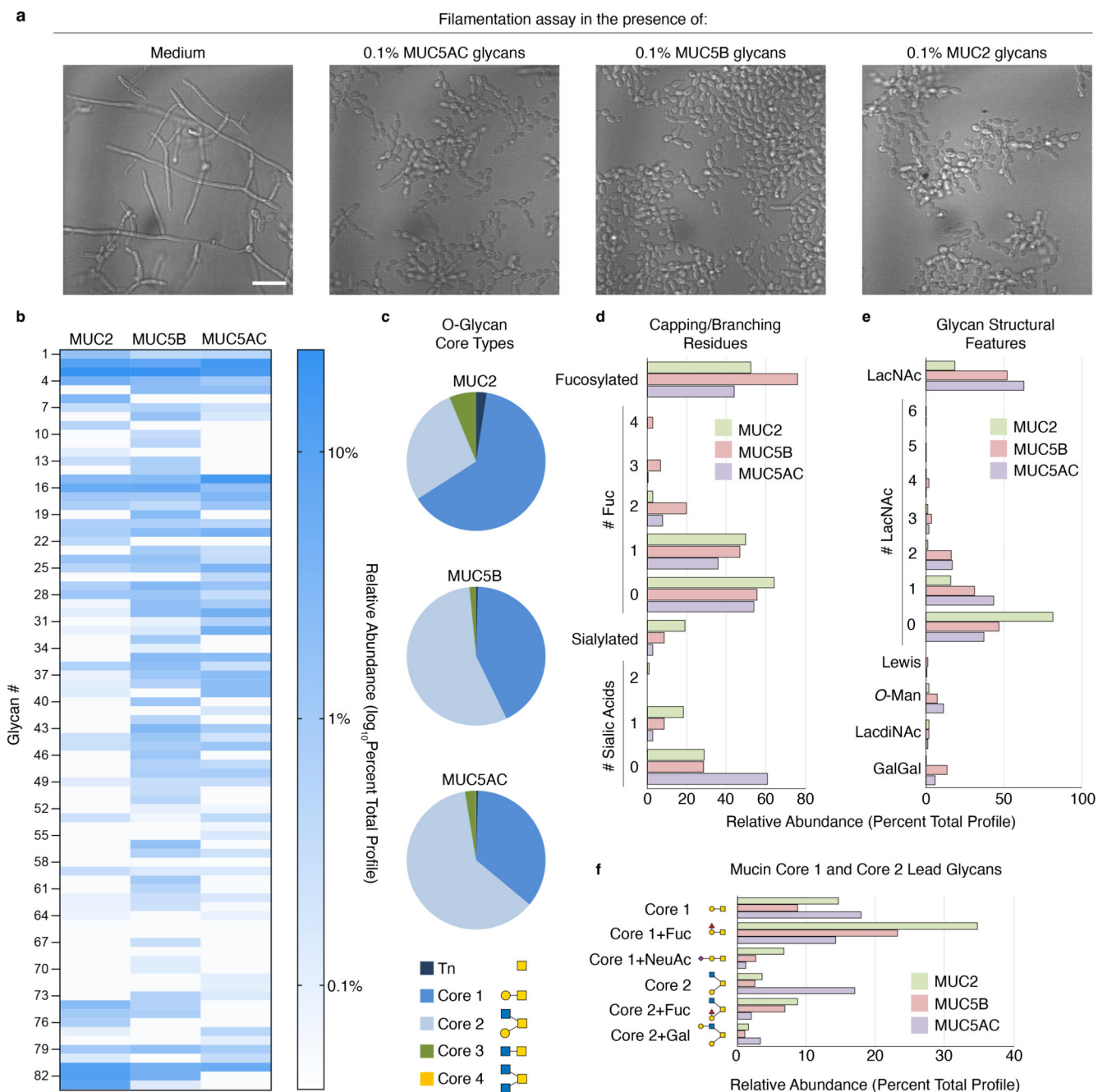


**Figure 5. Native mucins across microbial niches display a plethora of complex glycan structures with regulatory potential**

a) Wild-type *C. albicans* SC5314 cells were diluted into RPMI medium with or without mucin glycan libraries purified from MUC5AC, MUC2, and MUC5B and cultured at 37 °C for 8 h. Phase-contrast images of *C. albicans* revealed that mucin glycans across three mucin types suppress filamentation. Scale bar, 20  $\mu$ m.

b) Heatmap presenting  $\log_{10}$  values for the relative abundances of individual glycans released from the three mucins and detected by NSI-MS as permethylated derivatives (Supplementary Table 3). MUC2, MUC5B, and MUC5AC are dominated by *O*-GalNAc

Core 1 (glycans #3, 4, 5) and Core 2 derived glycan structures (glycans #15, 16, 17). Glycans #81, 82, and 83 represent non-reducing terminal disaccharides of incomplete core structures likely generated through peeling reactions during preparation.

- c) Distribution of *O*-glycans by GalNAc-initiated core type on each mucin. Minimal core structures are shown in the legend. The relative abundances of each glycan containing a minimal core structure was summed for comparison.
- d) The relative abundances of glycans carrying capping/branching fucose or sialic acid residues were summed for comparison across the three mucins. Glycans with between 0 and 4 fucose residues or between 0 and 2 sialic acid residues were detected. The relative abundances of sialylated and fucosylated glycans was calculated based on the total glycan profile, while the relative abundances of glycans lacking sialic acid or fucose was calculated based on the subset of glycans in the total profile that are structurally amenable to sialylation or fucosylation.
- e) The relative abundances of glycans that possess the indicated structural features or motifs were summed for comparison across the three mucins. Abbreviations for the features are as previously described (Fig. 2). The Lewis designation refers to the detection of a fucosylated LacNAc residue.
- f) The relative abundance of the six most prevalent Core 1 and Core 2 glycans shared across all three mucins is presented. These mucin-derived glycans defined structures that served as synthetic targets for generating lead compounds for subsequent functional analysis (Fig. 6).

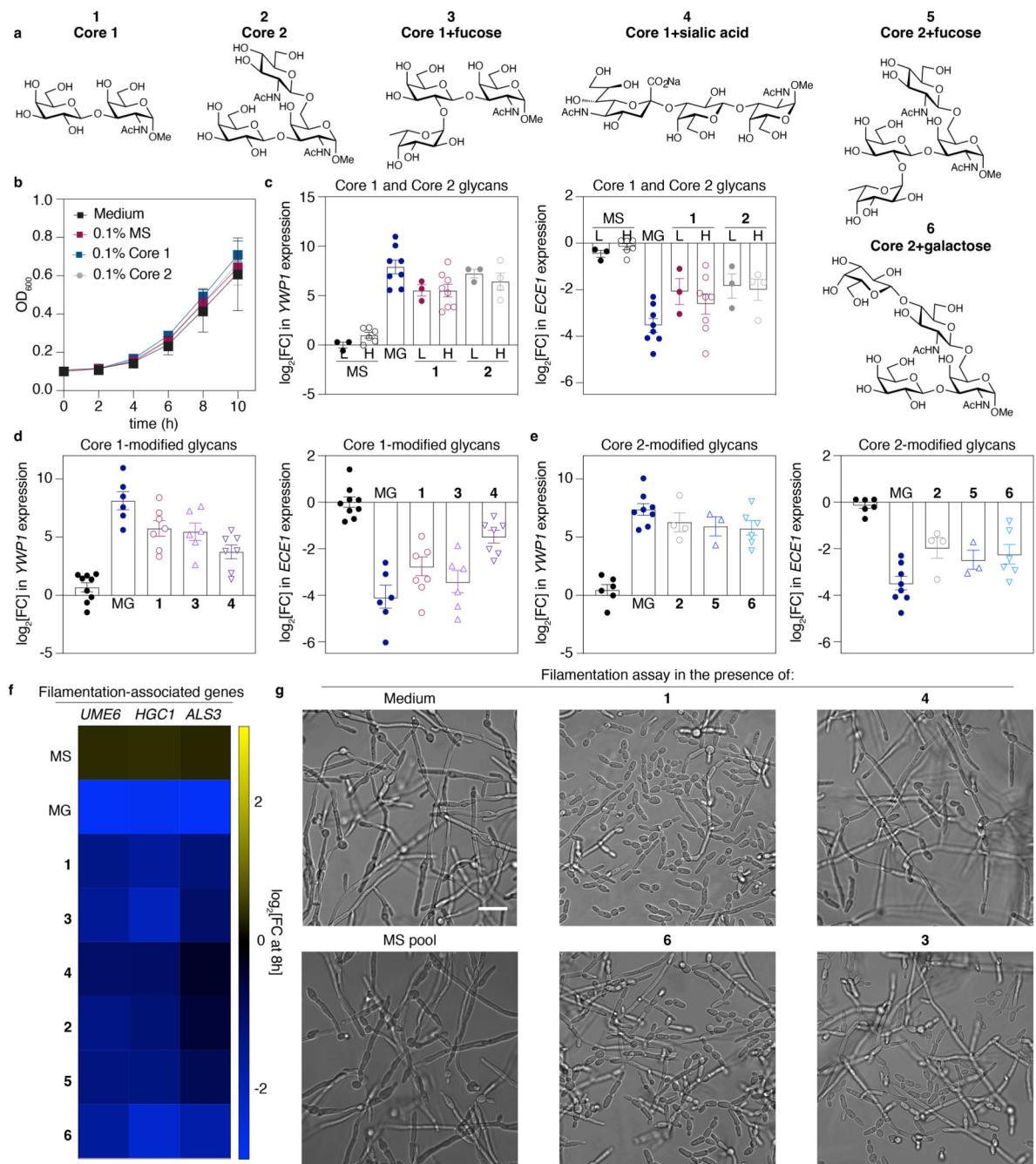


**Figure 6. Synthetic Core 1- and Core 2-modified glycans are sufficient to suppress *C. albicans* filamentation**

- a) Depiction of synthesized mucin glycan structures (1-6) that are abundant in the complex mucin glycan pool.
- b) Growth is not altered by the presence of the Core 1 and Core 2 synthesized glycans. Data are the mean  $OD_{600}$  measurements  $\pm$  SEM;  $n=5$  biologically independent replicates. MS, monosaccharide pool.

c) Exposure to low (L; 0.1% w/v) and high (H; 0.4% w/v) concentrations of synthesized glycan structures (left) increase transcription of the yeast-associated gene *YWPI* and (right) decreases transcription of the filamentation-associated toxin gene *ECE1*. Data from  $n=3$  (0.1% MS, **1** and **2**),  $n=4$  (0.4% **2**),  $n=6$  (0.4% MS) and  $n=8$  (0.1% MG, 0.4% **1**) biologically independent replicates.

d) Exposure to Core 1-modified glycan structures decreases the expression of the virulence-associated gene, *ECE1*, and increases the expression of the yeast-associated gene, *YWPI*. These results are dampened by the addition of sialic acid to Core 1. Data from  $n=6$  (MG, **3**),  $n=7$  (**4**, **1**) and  $n=9$  (MS) biologically independent replicates.

e) Exposure to Core 2-modified glycan structures decreases the expression of the virulence-associated gene, *ECE1*, and increases the expression of *YWPI*. Data from  $n=3$  (**5**),  $n=4$  (**2**),  $n=6$  (**6**, MS) and  $n=8$  (MG) biologically independent replicates.

f) Expression of filamentation-associated genes in the presence of MS, MG, and synthesized Core 1- and Core 2-modified glycan structures. Data indicates the mean from  $n=3$  (**6**),  $n=4$  (**3**, **5**),  $n=6$  (**2**) and  $n=7$  (MS, MG, **1**, **4**) biologically independent replicates.

g) Phase-contrast images of *C. albicans* SC5314 cells that were grown in RPMI medium alone, 0.4% monosaccharide (MS) pool or the indicated synthetic glycan structure (0.4%) at 37 °C for 8 h. Scale bar, 20  $\mu\text{m}$ .

For **c,d,e,f** gene expression was measured with qRT-PCR and normalized to a control gene (*ACT1*). Bars indicate mean  $\pm$  SEM. MS, black circles; MG, mucin glycans; FC, fold change.